1999

# Simulation of the formation and propagation of the thermal bar on Lake Ontario

Dilkushi Anuja de Alwis

# Simulation of the Formation and Propagation of the Thermal Bar on Lake Ontario

by

Dilkushi Anuja de Alwis

B.Sc., Mathematics and Computing, University of London. 1994

A thesis submitted in partial fulfillment of the
requirements for the degree of Master of Science
in the Chester F. Carlson Center for Imaging Science
of the College of Science
Rochester Institute of Technology

1999

Signature of the Author _____

Accepted by Henry E. Rhody 9/22/99

Coordinator, M.S. Degree Program Date

CHESTER F. CARLSON
CENTER FOR IMAGING SCIENCE
COLLEGE OF SCIENCE
ROCHESTER INSTITUTE OF TECHNOLOGY
ROCHESTER, NEW YORK

CERTIFICATE OF APPROVAL

---

M.S. DEGREE THESIS

---

The M.S. Degree Thesis of Dilkushi Anuja de Alwis
has been examined and approved by the thesis committee
as satisfactory for the thesis requirement for the
Master of Science degree

Dr. John R. Schott, Thesis Advisor

Dr. Anthony Vodacek

Mr. Rolando Raqueño

Dr. Alfred J. Garrett

9/22/99
Date

THESIS RELEASE PERMISSION

ROCHESTER INSTITUTE OF TECHNOLOGY

COLLEGE OF SCIENCE

CHESTER F. CARLSON

CENTER FOR IMAGING SCIENCE

Title of Thesis:

**Simulation of the Formation and Propagation of the Thermal Bar on Lake Ontario**

I, Dilkushi Anuja de Alwis, hereby grant permission to Wallace Memorial Library of R.I.T. to reproduce my thesis in whole or in part. Any reproduction will not be for commercial use or profit.

Signature _____ 22nd Sep 1999

Date

Simulation of the Formation and Propagation of the Thermal Bar on Lake Ontario

by

Dilkushi Anuja de Alwis

Submitted to the
Chester F. Carlson
Center for Imaging Science
College of Science
in partial fulfillment of the requirements
for the Master of Science Degree
at the Rochester Institute of Technology

## Abstract

Computer-based, mathematical models that simulate spatially distributed and time dependent environmental processes are increasingly recognized to provide diagnostic and productive outputs for the assessments of environmental factors. Mathematical models have been utilized since 60's to study the water quality, the circulation structure and the seasonal changes of large water bodies such as the Great Lakes. Analysis of changes in water quality related to seasonal cycles such as the formation and the propagation of the thermal bar requires spatial and temporal models, with high resolution. The overall objective of this study was to integrate geo-referenced site-specific spatial data to a 3D hydrodynamic model (ALGE) and compare the outputs with geo-referenced remotely sensed thermal imagery. The motivation of this work is based on the idea that the spatial data provides a significant advantage of equipping the model with site specific data to manipulate site specific circulation patterns. Further since the input is geo-referenced and site specific, the output can be directly compared to geo-referenced remotely sensed imagery for model validation. Thus, the aspect of integration of spatial data to hydrodynamic models is an obvious and promising approach to study lake-wide hydrodynamic processors and seasonal

changes. A specific objective of the study was to examine how different spatial patterns and weather conditions influence the formation and the propagation of the thermal bar temporally and spatially. Several preliminary studies were conducted on square lakes and lakes with false bathymetric profiles, and compared with the results of laboratory studies and field surveys. Since the outputs compared well with the literature, bathymetric data of Lake Ontario was integrated to the 3D hydrodynamic model with real time surface and atmospheric weather data. The formation and the propagation of the thermal bar was simulated for the years 1997, 1998, 1999 and 1997 (winter) through 1998(fall). The model was finetuned by changing the initial conditions and weather data to obtain a good approximation to the surface temperature derived from satellite imagery using the split and dual window technique. The lake was also subjected to different weather conditions to study its influences on the formation and propagation of the thermal bar. The model outputs from case studies as well as comparisons of the model output with satellite imagery and the NOAA forecasting model are discussed.

## Acknowledgements

I would like to express my sincere gratitude to my advisor Dr. John Schott for his priceless advice, guidance and inspiration from the start to the very end. I am of the opinion that it was a very wise decision for him to have decided to use ALGE as the hydrodynamic model for this study out of all the other hydrodynamic models available. It was Dr. Schott who made the above important decision, invited it's implementer Dr. Alfred Garrett (from DOE) to RIT to get me started on my thesis. Dr. Schott also found the financial resources to purchase the hourly weather data, satellite images and the necessary hardware for the study. He had a well defined task for me and his masterful instructions, wisdom and insight was instrumental in seeing the work successfully completed. He also worked on improving my presentation skills. It has been a pleasure and a privilege to have Dr. Schott as my advisor and to be able to be a part of his vision and the research team.

I would also like to thank Dr. Alfred Garrett(from DOE) for his unconditional support and his willingness to share his knowledge without any measure. From the day this study got off the ground Dr. Garretts support has been invaluable to the success of this work. He paid incredible attention to the details of my work and I am so thankful to him for not giving up on me. Dr. Garrett was always just an email away to provide assistance, support and encouragement.

I would also like to take this opportunity to thank my committee members Dr. Anthony Vodacek and Mr. Rolando Raqueño for taking the time to read over my thesis and provide valuable input and advice.

Ms. Nina Rolando Raqueño has been instrumental in providing me with the necessary spatial data in the GIS format. The DIRS/GIS spatial database that she has built throughout the years was a valuable resource. She was always there for me for support and guidance.

I would also like to thank Mr. Bryce Nordgren for providing me with the necessary computer workspace and providing me with the system administrative support.

It is difficult to give adequate thanks to all of the individuals from the DIRS team that, in the course of my endeavors, have provided assistance support and encouragement.

I would also like to thank The Fulbright Commission for supporting me financially.

Above all I would live to thank God for an opportunity to work on such an interesting piece of work and for all the supportive people who helped me along the way.

# Table of Contents

**List of Figures** x

**1 Background** 2
- 1.1 Introduction . . . 3
  - 1.1.1 Problem Definition . . . 3
- 1.2 The Great Lakes . . . 7
- 1.3 Laboratory Studies of the Thermal Bar . . . 12
  - 1.3.1 Experimental Setup . . . 13
  - 1.3.2 Heating Techniques . . . 14
  - 1.3.3 Measurements . . . 15
  - 1.3.4 Experiments . . . 16
  - 1.3.5 Observations . . . 17
  - 1.3.6 Discussion . . . 19
- 1.4 Field Investigation and the use of Satellite Imagery to Study the Thermal Bar 21
  - 1.4.1 Potential of Remote Sensing(Schott, 1982) . . . 21
  - 1.4.2 Using HCMM Satellite Images to Study the Formations of the Thermal Bar on Lake Ontario (Schott, 1982) . . . 22
  - 1.4.3 Use of Regular IR Satellite Data to Investigate Thermal Bar and Upwelling Phenomenon (I. A. Bychkova and Demina, 1989) . . . 23
  - 1.4.4 Documentary Complex Surface Temperature Patterns from AVHRR Imagery of Sagniaw Bay.(J. W. Budd and Maclean, 1998) . . . 26
  - 1.4.5 Field investigation of the Thermal bar in Lake Ontario (Rodgers, 1971) 29
  - 1.4.6 Methods of Observation . . . 30
  - 1.4.7 Results and Analysis . . . 31

**2 Theory** 33
- 2.1 Sea Surface Temperature Measurements from Space . . . 34
  - 2.1.1 Blackbody Radiation . . . 34
  - 2.1.2 Estimation of Temperature . . . 35
  - 2.1.3 Sea Surface Temperature Algorithms . . . 36
- 2.2 ALGE- The 3D Hydrodynamic Model (Garrett, 1997) . . . 41
  - 2.2.1 Hydrodynamic Equations . . . 41

2.2.2 Mixing Parameterizations . . . . . 43
2.2.3 Energy Transfer . . . . . 44
2.2.4 Boundary Conditions . . . . . 48
2.2.5 Land-Water Distribution . . . . . 49
2.2.6 Surface Meteorological Data . . . . . 49
2.2.7 Upper Air Meteorological data . . . . . 50
2.2.8 Tidal Forcing . . . . . 50
2.2.9 Water Depths . . . . . 51
2.2.10 Other Input Parameters . . . . . 51

**3 Approach and Results** **52**
3.1 Comparison of ALGE with satellite images and other hydrodynamic models 53
3.1.1 Comparison of ALGE with satellite images . . . . . 53
3.1.2 Comparison of the split and dual window techniques . . . . . 53
3.1.3 Comparison of Split and Dual window technique with the IMGMAP and OCNMAP algorithms . . . . . 55
3.1.4 Comparison of ALGE output with surface temperature derived from satellite imagery . . . . . 56
3.1.5 Comparison of ALGE with the NOAA forecasting model . . . . . 58

**4 Conclusions and Recommendations** **60**
4.1 Recomendations . . . . . 61

**A ALGE code** **64**

**B The contents in the attached CD** **102**

# List of Figures


1.1 Relief, Dranage and Urban Areas (K Fuller and Witting, 1995) . . . . . 7
1.2 Wind set-up is a local rise in water caused by winds pushing water to one side of the lake (K Fuller and Witting, 1995) . . . . . 9
1.3 The Great Lakes Water System (K Fuller and Witting, 1995) . . . . . 10
1.4 Laboratory setup (Elliott and Elliott, 1970) . . . . . 14
1.5 Figure 1 A temperature subsection from the heated "spring" system Figure 2 A temperature subsection from the cooled "Fall" system (Elliott and Elliott, 1970) . . . . . 18
1.6 Bathymetric profile of Lake Ladoga (Malm and Jonsson, 1993) . . . . . 23
1.7 Movement of the Thermal bar on Lake Ladoga as indicated by satellite IR data . . . . . 24
1.8 Propagation of the thermal bar on Lake Ladoga . . . . . 26
1.9 Location map of Sagniaw Bay, Lake Huron. NOAA/GLERL sampling locations are numbered 1 to 26 . . . . . 27
1.10 Field investigation of the Thermal bar in Lake Ontario : Sampling locations and survey dates . . . . . 30
1.11 Heat content changes along Line C relative to surveys 1 to 12 - March $9^{th}$ to June $22^{nd}$1970 . . . . . 32

2.1 Blackbody curves and solar exitance spectra (Schott, 1997) page 61 . . . . 35

3.1 Comparison of the Split and Dual window algorithms for June 09 1997 . . . 54
3.2 Comparison of Split window technique with the IMGMAP and OCNMAP algorithms April 28 1998 . . . . . 55
3.3 Comparison of Split window technique with the IMGMAP and OCNMAP algorithms - June 01 1998 . . . . . 56
3.4 Comparison of ALGE output with surface temperature derived from satellite imagery - April 27 1998 . . . . . 57
3.5 Comparison of ALGE output with surface temperature derived from satellite imagery - June 04 1998 . . . . . 57
3.6 Comparison of ALGE output with surface temperature derived from satellite imagery - July 11 1998 . . . . . 57

3.7 Comparison of ALGE output with surface temperature derived from satellite imagery August 09 1998 . . . . . 58
3.8 Comparison of ALGE with the NOAA forecasting model- Date $7^{th}$ April 1998 59
3.9 Comparison of ALGE with the NOAA forecasting model $15^{th}$ July 1998 . . 59

## 1.1 Introduction

### 1.1.1 Problem Definition

Computer-based, mathematical models that realistically simulate spatially distributed and time dependent environmental processes are increasingly recognized to provide diagnostic and predictive outputs for the assessment of environmental factors. Mathematical models have been utilized to study and characterize water quality and movement since the early 60s. In fact several physical models in the form of tanks were used in the late 60s to study circulation structure and seasonal changes such as the thermal bar. Elliott and Elliott (1969,1970) and Kreyman (1989) have carried out experimental studies of the thermal bar. The thermal bar is a naturally occurring process in many lakes, including the five Great Lakes. It results from the transition from winter stratification, where the coldest water in the lakes moves from the surface to the bottom. During the turnover, spring rains, spring runoff and snow melt, warm the lake at the edges. As the water mixes to $4^oC$ the maximum density of water, it sinks, forming two circular currents within the lake. Despite the absence of Coriolis effects those experiments were able to reproduce many of the features of the thermal bar observed in the field. Most theoretical studies of the thermal bar have concentrated on modeling the dynamics associated with the formation and the propagation of the thermal bar. Elliott and Elliott(1970) developed a two dimensional model which ignored the horizontal transport of heat, from which they obtained the positions of the thermal bar as a function of position. Zilitinkevich, Kreiman and Terzahevik (1992) described a more complex model that allowed for the horizontal transport of heat from the warm, shallow regions into the vicinity of the thermal bar thereby increasing its propagation speed. Elliott (1970) developed a model for the circulation associated with the thermal bar by assuming a balance between vertical shear and the horizontal pressure gradient. Bennett (1971) carried out a numerical investigation of the thermal bar. Bennett's model was fully three dimensional ($3D$) and included rotational effects. The results predicted

that the motion was largely confirmed due to the warm near-shore, region and that the flow would be geostrophically balanced (Farrow, 1995). Farrow(1995) also concluded that horizontal heat transport could be important in the shallow regions but that there appeared to be no significant heat transport into the isothermal region- thermal bar. Farrow(1995) presented an asymtotic solution (based on small bottom slope) for an idealized model for the thermal bar phenomenon in the non-rotating frame that included initial effects. In a departure from the heat balance or general circulation models, Kay, Kuiken and Merkin (1995) examined the detail of the downwelling region of the thermal bar (Farrow, 1995). The steady state boundary layer analysis yielded the vertical velocity and temperature structure in the plume as well as the horizontal velocity induced in the far field. The thermal bar prevents the natural mixing of water causing the higher concentration of nutrients and pollutants coming off the land to remain near shore rather than distributing evenly over the entire body of water. This process is likely to have critical impacts on the ecosystem of the lake basin. Current analysis of water quality related to seasonal cycles specially due to the formation and the propagation of the thermal bar require a more detailed knowledge of velocity components at any location of the lake. Thus, the development of a spatial and temporal model, capable of providing more precise resolution is a challenging task for water quality studies in lakes. The rapid development of spatially distributed models are replacing simple spatially aggregated or lumped parameter models. This is due to the availability of more powerful computing devices and supportive software. Also regardless of the level of computational sophistication the site specific data is capable of emphasising the specific hydrodynamic lake-wide spatial patterns.

### Objectives

The overall objective of this study was to integrate geo-referenced site specific spatial data to a 3D hydrodynamic model and compare the outputs with geo-referenced remotely sensed thermal imagery. The motivation of this work is based on the idea that the spatial data

provides a significant advantage of equipping the model with site specific data to manipulate site specific circulation patterns. Since the input is geo-referenced and site specific, the output could be directly overlaid over geo-referenced remotely sensed imagery for comparison and feature extraction of regions of interest. Thus, this aspect of integration of spatial data to hydrodynamic models is an obvious and promising idea to study lake-wide hydrodynamic processes and seasonal changes. Specific objectives of the study are to examine how different spatial patterns including the weather conditions influence a seasonal formation and propagation of the thermal bar. This study also examines the effects of model spatial resolutions and its impact on the output. The inputs used in this study have spatial context. In addition to gaining insight into the formation and propagation of the thermal bar, this study demonstrates the capabilities of hydrodynamic models. The output of the study were compared with satellite thermal imagery derived from the split and dual window technique and with another hydrodynamic model.

### Overview of the Study Approach

ALGE is a 3D hydrodynamic model developed by Dr. A. Garrett of the Department of Energy (Garrett, 1997) is used to study the formation and the propagation of the thermal bar. The code has been used to predict the temperature distributions in lakes, rivers and cooling ponds but has not been used to simulate dimictic lakes before. Hence several case studies were conducted on square lakes to study the seasonal changes such as the formation and the propagation of the thermal bar. The results were compared to that of the laboratory experiments, literature and models on the thermal bar. Since the main objective of the study was to integrate spatial data to the hydrodynamic model, spatial data (bathymetric data) in the shape of Lake Ontario was integrated to the model. Several case studies were conducted varying different parameters such as the temperature at which the lake becomes stratified, the cloud cover, the wind speed etc. All the above showed satisfactory results, hence it was decided to integrate real bathymetric data of Lake Ontario

obtained from the DIRS-GIS (Digital Imaging and Remote Sensing Laboratory- Geographic Information Systems). Several case studies were conducted to investigate how sensitive the model was to the weather data, bathymetric grid resolution (vertical and horizontal), spatial location of the weather station and integration of the inflow and outflow. The formation and the propagation of the thermal bar was investigated for the years 1997, 1998 and 1999. The above simulation was also executed from the beginning of 1997 to the end of 1998, for a period of one and a half years. The simulation output has been compared to surface temperature maps derived from the split and dual window techniques and other model outputs. A summery of the previous studies of the thermal bar from the laboratory simulations to the satellite imagery studies and field surveys are discussed in the following chapters. The theory and the numerical equations used in the simulation are summarized along with the theory involved in deriving the surface temperature from AVHRR imagery using the split and dual window techniques. Chapter 2.2 discusses the simulation code (ALGE) in detail and explains the output parameters. A step through the detailed case studies conducted on the above model and the observations are also discussed.

## 1.2 The Great Lakes

The largest system of fresh water on planet Earth, the Great Lakes spans more than 1,200 kilometers (750 miles) from West to East providing water for consumption, transportation, power, recreation and a host of other uses. The lakes contain about $23,000Km^3$ (5,500 cu. miles) of water and is about 18 percent of the world supply of fresh surface water (K Fuller and Witting, 1995). Although the Great Lakes is a part of a single system it comprises five lakes namely Superior, Michigan, Huron, Erie and Ontario.

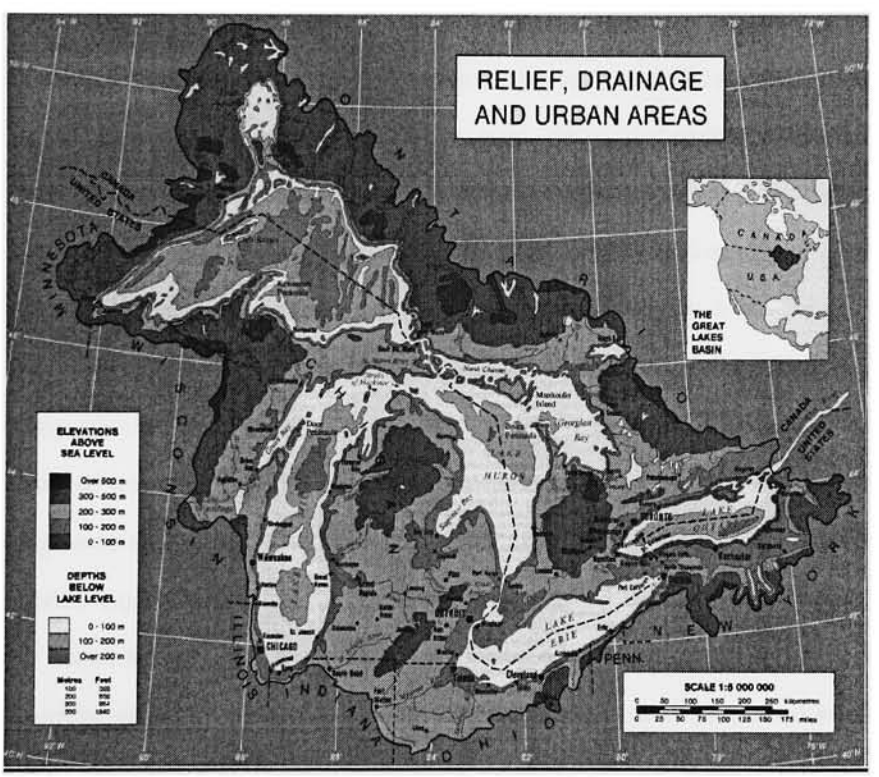


Figure 1.1: Relief, Dranage and Urban Areas (K Fuller and Witting, 1995)

Because of the large size of the water shed, physical characteristics such as climate, soils and topography vary across the basin. To the North the climate is cold and the terrain

is dominated by granite bedrock while the southern area of the basin is much warmer and the soils are deeper with layers of mixtures of clays, silts, sands. The prevailing movement of air is from the west and the characteristically changeable weather of the region is due to the alternating flows of warm, humid air from the Gulf of Mexico and cold dry air from Arctic. Most of the moisture in the Great Lakes basin is evaporated water from the surface of the five lakes. The water that evaporates contains dry air forming vapor. The vapor, contribute to the humidity of the atmosphere or it condenses and forms water droplets, which form fog and clouds. Moisture-bearing air masses enter the Lake basin due to the global movement and deposits rain, snow, hail or sleet which is stored as fresh water. The precipitation that falls on land becomes surface runoff or ground water.

In the fall and winter months, release of the heat stored in the lakes during the summer, moderates the climate near the shores of the lakes. Also the cold and dry air from the Arctic enters the basin, but is warmed and picks up moisture travelling over the comparatively warmer lakes. Less frequently, slightly warmer and more humid air masses enter the basin from the Southwest, bringing in moisture from the Gulf of Mexico. During the winter, the temperature of the lakes continue to drop, in autum, the rapid movement and occasional clash of warm and cold air masses through the region produce strong winds. Air temperature begins to drop gradually and less sunlight, combined with increased cloudiness, signal more storms and precipitation. Spring in the great Lakes region, like autumn, is characterized by alternating air masses moving through rapidly, resulting in frequent cloud cover and thunder storms. By early spring, the warmer air and increased sunshine begin to melt the snow and like ice, creating thermal layering of the lakes. The lakes are slower to warm than the land and tend to keep adjacent land areas cool, well into summer (K Fuller and Witting, 1995)

As the westerly winds continuously carry moisture into the basin, the basin loses moisture by evaporation and transpiration and through the outflow of the St. Lawrence river. The day to day changes in lake level are caused by the wind setups are usually associated

with major lake storms that last for hours or days. Also the barometric pressure along with rapid changes in winds causes the water to oscillate which is commonly known as 'Seiche'. The water levels in the lakes change annually and seasonally due to the change in precipitation and runoff to the Great Lakes.

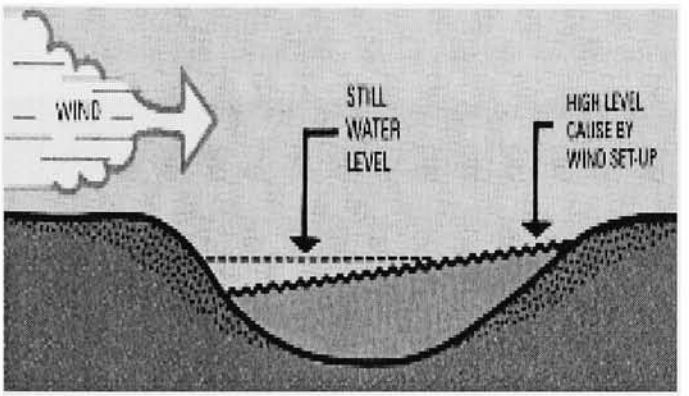


Figure 1.2: Wind set-up is a local rise in water caused by winds pushing water to one side of the lake (K Fuller and Witting, 1995)

Outflow from the Great Lakes is relatively small (less than 1 percent per year) in comparison with the total volume of water. Pollutants that enter the lake - whether by direct discharge along the shores, through tributaries, from land use or from the atmosphere- are retained in the system and become more concentrated with time.

The sources of pollution include the runoff of soils and farm chemicals from agricultural lands, the waste from cities, discharges from industrial areas and leachate from disposal sites. The large surface area of the lakes also makes them vulnerable to direct atmospheric pollutants that fall with the rain or snow and as dust on the lake surface. Surface runoff is a major source of pollution due to the soil sediment deposition and also aggravates flooding problems. Groundwater is important to the Great Lakes as it acts as a reservoir for collecting and storing water and slowly replacing the lakes, directly or indirectly as base flow to the tributaries.

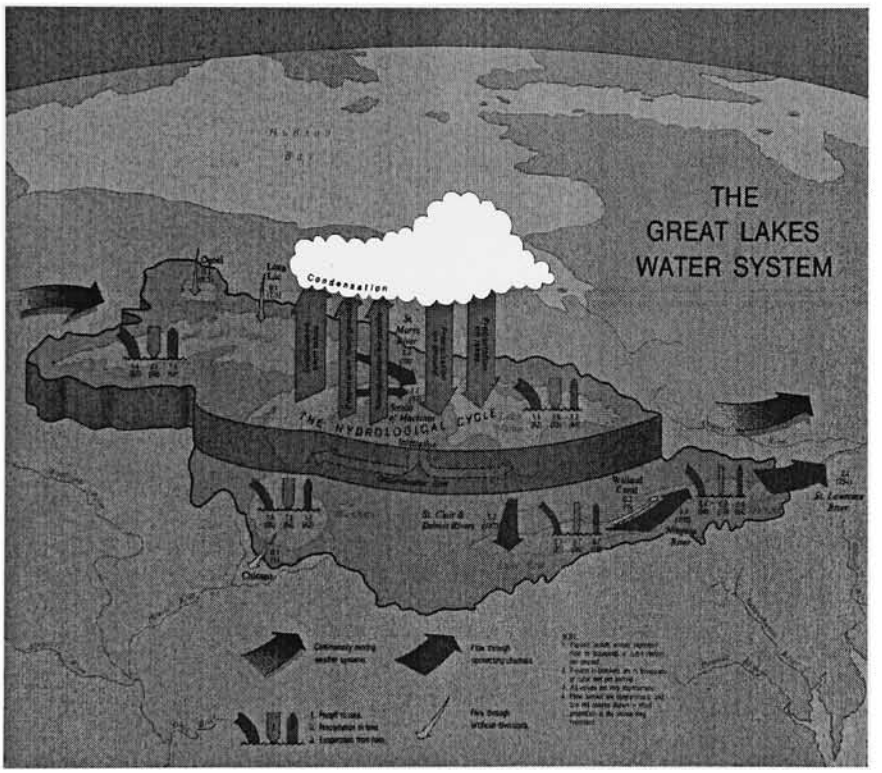


Figure 1.3: The Great Lakes Water System (K Fuller and Witting, 1995)

## 1.3 Laboratory Studies of the Thermal Bar

The Great Lakes are a highly dynamic system with a variety of subsystems that change seasonally and on longer cycles. Stratification which is a layering of water in the lakes is caused due to the change of the density of water. Hence the lake tends to have distinctive surface layers specially in the area close to the shore. The density of water increases as the temperature decreases until it reaches it's maximum density at around 4 degrees Celsius. Also in the colder water (temperature less than 4 degrees Celsius) the density increases as the Temperature increases until 4 degrees Celsius.

In Spring the long wave and short wave heat radiation passing from the atmosphere to the water heats up the lake. The amount of heat is determined by the meteorological factors. As the water is most dense at 4 degrees Celsius, it increases the gravitational force acting on the water which makes the water sink. This downward motion of the particles forms a screen that separates out the warmer shallow region from the deeper colder region. This sinking isothermal zone which separates the lake into two cells of warmer and colder zones is known as the Thermal Bar. The shallow warmer cell tends to be horizontally stratified while the colder deeper region gets vertically stratified. Therefore the stratification of density on both sides of the isothermal region that corresponds to maximum density appears to show opposite behavior: hydrostatistically stable in the Shallow zone and unstable in the deep-water zone.

As time progresses from winter to spring the near-shore region temperature becomes large enough that a cross shore density gradient is created. This results in a pressure difference which tends to push the warm water offshore to the center of the lake. This is known as the propagation of the Thermal bar.

The propagation of the thermal bar proceeds until the colder deeper region reaches the temperature of the thermal bar, which causes the lake to turn over completely. A similar phenomenon is observed during fall when the shallow near-shore zone gets cooler faster than

the deep-water zone. The colder water becomes denser and descends displacing deep waters and causing a mixing or turn over. As the warm lake gets colder and reaches a temperature of 4degrees Celsius the Thermal bar is formed and the thermal bar propagates from the center of the lake to the lake shore.

The annual layering and the turnover of water are important for the water quality of the lake. Since the turn over is the main way in which oxygen-poor water in the deeper areas of the lake can be mixed. This prevents anoxia or complete oxygen depletion of the lower level of the most of the lakes.

The thermal bar phenomenon has been studied in a quantitative manner using laboratory models. Such studies have been described by (Elliott and Elliott, 1969) (Elliott and Elliott, 1970) and (Kreyman, 1989).

(Elliott and Elliott, 1970) studied the effects of variation of heat input, bottom slope and initial temperature on the propagational speed of the thermal bar. The results of the above model was compared with the results of Lake Ontario.

(Kreyman, 1989) studied the shifting of the warm region varying the kinetic heat-flux, initial temperature and the bottom slope.

### 1.3.1 Experimental Setup

(Elliott and Elliott, 1969) and (Elliott and Elliott, 1970) used a tank $1.5m$ long and $30cm$ wide with the maximum depth of $27cm$. The long walls were a double thickness of $0.6cm$ plexiglass separated by $1.2cm$ air space. The end walls and bottom was plywood with styroform insulation. An arbitery slope of five degrees were chosen as being small and yet reasonable for the length of the tank. This resulted in the depth going from zero at one end to approximately 13cm at the other end. The tank was filled with fresh tap-water with ice of liquid detergent to remove the tension effects when addition of dye to observe currents. Crushed ice was stirred into the water to lower the temperature of the water to near $0^oC$ and then excess ice was removed and mean temperature measured.

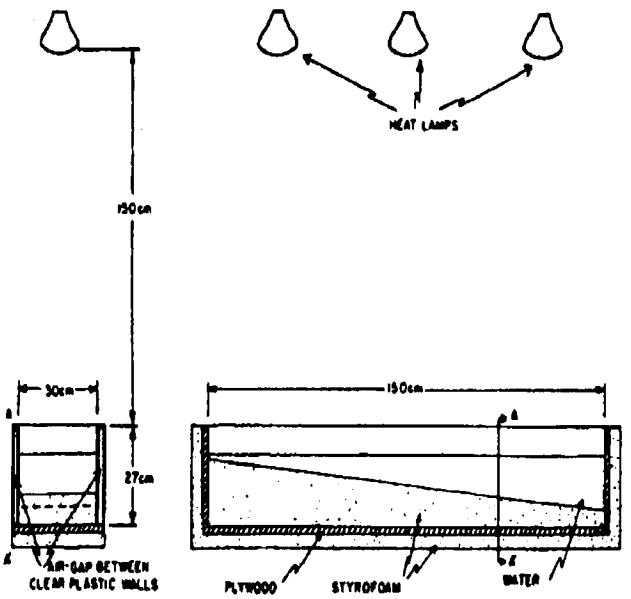


Figure 1.4: Laboratory setup (Elliott and Elliott, 1970)

(?) used a $140cm$ by $40cm$ tank made of wood and a constant slope of $6^o10$. The slope was made such that the depth of the basin increased uniformly in the longitudinal direction from 0 at one end to 15.7 cm at the opposite end. The basin was filled with tap-water then ice added which made the mean water temperature to be less than $4^oC$.

### 1.3.2 Heating Techniques

(Elliott and Elliott, 1969) and (Elliott and Elliott, 1970) heated the tank with three heat lamps equally spaced with respect to the tank at $1.5m$ above the surface. The lamps were arranged to give a roughly uniform heat source over the surface. Elliot & Elliot (1970) used a relatively higher heating rate using 5 heating lamps. The water was heated by long wave radiation and heat conduction through the walls. Using three lamps the heating rate was about $9 \times 10^{-3} cal/cm^2/sec$ of this $2 \times 10^3 cal/cm/sec$ through the walls.

(Kreyman, 1989) used 5 electric bulbs with normal output of $200W$ which were placed on a special stand uniformly along the basin above the water surface. In order to vary the heating conditions the strength of the current in the circuit for the light source and their distance from the water were varied from experiment to experiment from $160 - 230W$ and from 0.8 to $1.1m$. Which in-return varied the heat flux in the range from $3 \times 10^3$ to $6 \times 10^3 kcm/s$ on to the surface of the tank.

### 1.3.3 Measurements

(Elliott and Elliott, 1969) made measurements of both current and temperature using Rhodamine B dye to make vertical dye traces. Both visual and time-lapse photography were used to investigate flow patterns. (Elliott and Elliott, 1970) obtained temperature profiles using a thermistor bead (VECO $32A5$), attached to the end of a $40cm$, thin glass rod with centimeter markings, which was lowered vertically through the water. The resistance of the thermistor was measured directly with a Fairchild Multimeter (Model 7050). The current structure was observed by dropping flakes of Rhodamine B dye along the transparent sides of the tank. These flakes sank to the bottom leaving vertical red traces. These dye traces were positioned with respect to a centimeter grid on a blank wall and their relative motions were obtained from time series photographs and from $16mm$ movies of the dye streaks.
(Kreyman, 1989) measured the water temperature using a vertical probe with a $M7 - 54$ sensor and was recorded using the $KSP4$ recorder. The measurements were made in longitudinal subsection passing through the middle of the basin. The distance between neighboring points at which the temperature were taken decreased from $10cm$ in the horizontal non-uniform regions to $2.5cm$ in the zone of the thermal bar. Potassium-Magnanese Oxide crystals were used to study the circulation patterns in the basin.

### 1.3.4 Experiments

(Elliott and Elliott, 1969) simulated the spring or heating period by first cooling the waters in the tank down to $0^oC$ using crushed ice and heating the tank with heat lamps. Experiments were done varying the slope in the tank by (Elliott and Elliott, 1970). Three slopes were used $(2.5^o, 5^o, 7^o)$ for different initial temperatures and different heat flux from the surface. A simple linear model was used to evaluate the speed of the bar with the above variables. The model is based on the assumption that horizontal advection and diffusion of heat are not of primary importance.

The bar speed is defined as the time taken to heat a column of unit area at a point P at the center of the tank upto $4^oC$. The model calculates the speed of the bar S as,

$$S = \frac{QL}{\triangle T \rho C_p D}$$

$Q$ : Flux through the surface in $cal/cm/sec$

$L$ :the distance from the shallow region to the point P

$D$ :depth at point P

$\rho$ :density

$C_p$ : specific heat

Hence given the main temperature at $P$ and the distance to the point $P$ from the present position of the thermal bar the time taken for the thermal bar to reach the point $P$ can be calculated.

The bar speed was measured by varying the slopes and the amount of heat flux through the surface. At one stage of the experiment an insulating lid was put on the tank which proved a strong dependence of speed on the surface heat input rather than on the horizontal density gradient or on other heat transfers (Elliott and Elliott, 1970).

(Kreyman, 1989) carried out six experiments by varying the initial temperature of the water in the tank and the surface heat flows passing through the free surface. The distance from the acute edge of the wedge to the line for the bar, i.e. the extent of the thermal

region, at successive points in time were calculated using

$$L = \frac{Q_s t}{\mu(T_m T_o)}$$

Where t is the time from the start of heating $\mu = \alpha g$ where $\alpha$ is the slope of the bottom surface and $T_o$ is the initial temperature $T_m$ is the temperature at which the water has its maximum density. The extent l of the warm region were plotted of different heat fluxes from the free surface varying from $3.3Kcm/s$ to $5.9Kcm/s$.

### 1.3.5 Observations

(Elliott and Elliott, 1969) observed the heating and the cooling temperature current patterns in isothermal regions. Isotherms were drawn for the temperature values from $3.5^oC$ and $4.5^oC$. Although actual maximum is at $4^oC$ the density of $3.5^oC$ and $4.5^oC$ water is only $2x10^{-6}g/cm^3$ lower. It was observed that the first order sinking occurs in the region between the above isotherms.

The dye traces were put in once the bar had a chance to form properly and water current were observed. A thermocline developed on the shallow side due to the penetration of heat energy and molecular thermal conduction, but in nature the mixing would be the main reason. On the other deep side the upper water was observed to move towards the bar and then sink. The approximately constant position of the lower boundary of the tongue of warm water, which was moving towards the bar, was maintained by a slow upward flow from the lower water. No contribution to the sinking from the warm side of the bar to the cool side was observed. Vertical temperature stratification near the surface was seen on the deep side of the 'bar.

(Elliott and Elliott, 1970) plotted the position of the thermal bar along the tank vs. the time and compared it to the linear mathematical model. It was observed that the model gives a good first approximation to the heat content along the tank. The physical model was also compared with lake Ontario. The net surface heat transfer at the surface of the

lake was assumed to be constant and a value of $7x10^{-3}cal/cm^2/sec$ (typically experienced in spring). The calculated values for the speeds of the propagation of the thermal bar were $0.95cm/sec$ (North shore) and $0.3cm/sec$ (South Shore). The predicted values were 0.7 and 0.4 respectively.

The difference in the above could be due to the assumption of negligible horizontal advection and diffusion. In both cases, in the deeper regions most of the heat is carried by convective processes. The advection of warm water towards the bar in the shallow end is not prominent in the tank. The tank flow is found to be less at shallow bottom slopes.

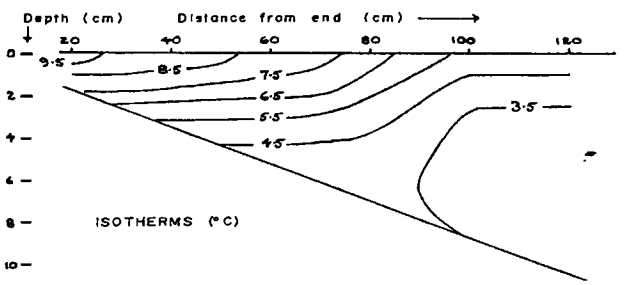


FIG. 1. A temperature section from the heated "spring" system.

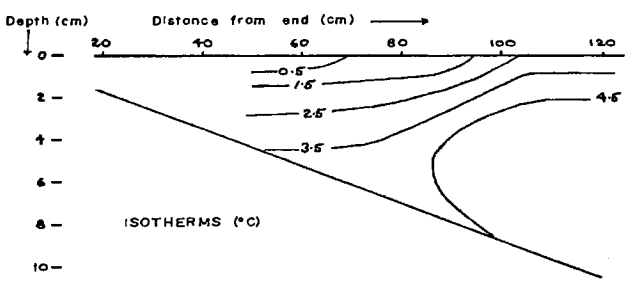


Figure 1.5: Figure 1 A temperature subsection from the heated "spring" system Figure 2 A temperature subsection from the cooled "Fall" system (Elliott and Elliott, 1970)

K. D. Kreyman, states that the temperature surveys showed that 6 to 8 minutes after heating of the water began there was a clearly observed warm shallow-water zone above the temperature of $4^oC$. The boundary between the heated and cold water was clearly defined

by the characteristic orientation of the isotherms. In the warm region the isothems were arranged nearly horizontally with a small slope toward shallow-water side and in the cold region they were arranged vertically.

In the warm region of the wedge the water temperature decreased exponentially with depth. The tracer observations showed the closed circulation systems with horizontal axes oriented along the bar line developed separately in the warm and cold regions.

It was also noted that as the thermal region increased, the frontal subsection, moving toward the deep part of the basin took on an inclined position and was distorted. During the first phase of the experiment $l \sim t$, after 30 to 35 minutes, when the warm region encompassed 0.5 $0.7m$ accelerated and corresponded more to the relation $l \sim t^{\frac{3}{2}}$. During the above accelerating the amount of heat flux was kept constant.

### 1.3.6 Discussion

(Elliott and Elliott, 1969) compared the observations of the tank to the field observations. There were several obvious similarities. There was a motion toward the bar on the shallow side as (Rodgers, 1971) calculated. There was no horizontal motion in the upperlayer of the bar. Thus the tank experiment appears to present a reasonable model of the natural phenomenon observed in the great Lakes.

(Malm and Jonsson, 1993) suggests that a lake cannot be considered to have a uniformly sloping bottom hence the relation to the depth instead of the slope is a better assumption. Accordingly

$$D = \frac{Qt}{\rho C_p (T_m T_o)}$$

would be better.

The above could be used to determine the existence of the thermal bar in a day by integrating the average heat flux and the average depth. It was stated by (Malm and

Jonsson, 1993) that if the heat flux $Q(t)$ changes with time the simple dynamics of the above equation does not apply.

It could also be concluded that the model results are rather sensitive to the initial temperature $T_o$. The higher the value of $T_o$ is the higher the thermal bar progression rate will be. For instance, if $T_o = 0.5^oC$ the thermal bar progression rate will be 12% higher than $T_o = 0^oC$.

## 1.4 Field Investigation and the use of Satellite Imagery to Study the Thermal Bar

### 1.4.1 Potential of Remote Sensing(Schott, 1982)

Most studies of the thermal bar phenomenon have been either detailed studies of a certain region or lake as whole. Since the thermal bar is prominent in large lakes, the diversity of the lakes make it difficult to apply detailed studies to the entire lake. Aerial satellite remote sensing offers a potential tool for lake wide sampling combined with considerable localized details (Schott, 1982). Remote sensing offers an ability to monitor the surface water temperature over the entire lake. Haynes and Wipple :1971 were among the first to demonstrate that aerial infrared line scanners could be used to map variations in the temperature of surface waters (Schott, ). Scarpace et.al., 1974 demonstrated that aerial infrared images could be quantified through the use of simultaneous surface measurements. Strandberg, 1967 discussed how variations in water quality can be observed using air-borne photographic systems. Lillesand et.al.,1973 took this a step further demonstrating that the concentration of suspended solids in a water body could be computered from densitometric analysis of air photos. Johnson, 1978 has demonstrated that chlorophyll concentrations could be studied using similar ground truth sampling correlated with aerial data (Schott, ). All the above approaches used ground truth to calibrate images. In order to overcome the limitations of ground truth sampling a statistical model was used to derive water quality parameters. Piech et.al.,1978 and Schott, 1980 developed a technique where aerial photographs or satellite images were processed through statistical models to derive the reflectance of different water containing coloring agents such as chlorophyll, suspended solids and yellowing organics. The output of the model showed a significant change in reflectance due to the quality of water.

### 1.4.2 Using HCMM Satellite Images to Study the Formations of the Thermal Bar on Lake Ontario (Schott, 1982)

The experimental approach in the above study was to obtain aerial thermograms during the satellite overpass. Which were used as ground truth points to calibrate the satellite images as suggested by Schott and Schimminger, 1981. The calibration accuracy using this approach was demonstrated to be within $1.1^oC$ of actual surface values. The isothermal maps were used to study the formation and the propagation of the thermal bar on Lake Ontario. In addition to studying the week-to-week development of the thermal bar, the diurnal coverage of the HCMM satellite permitted mapping of 12 hour advances of the thermal bar. This enabled the study of the day-night temperature differences and the advances of the thermal bar within that time. The bulge created by the Niagara plume was clearly seen in the above study until the thermal bar advanced beyond the influence of the plume. Aerial color photographs were used to study the water quality especially near the thermal bar. The approach is a conversion of density measurements on the photographic records to the volume spectral reflectance of the water. Once the spectral reflectance values of the water are known, the dominant water quantity change could be determined. To obtain a more synoptic evaluation of water quality brightness vectors of the red to green channels of LANDSAT satellite were used for a portion of Lake Ontario. The brightness vector measured the overall turbidity of the water which directly indicates the concentration of algae and suspended particles in the water. Warm nutrient-rich water trapped in shore in the thermal bar was clearly seen in the water quality images derived from the LANDSAT data. The effects of the thermal bar on water quality was studied in detail in the above study using HCMM satellite day-night overpass imagery and water quality data collected by the Canada Center for Inland Waters(CCIW). The CCIW collected the surface temperature, secchi depths and integrated chlorophyll at several points of interest on the lake. The ground truth was used to verify the interpolation of the auxiliary LANDSAT and underflight data relative to water quality. The CCIW showed a definite increase associated with dramatically

elevated chlorophyll levels occurring in shore of the thermal bar. Suspended solids and other factors affecting water color were not a part of CCIW's analysis. The above study clearly states that the HCMM sensor combined with other aerial and space-borne sensing systems offers a way to monitor the location of the thermal bar and its impact on water quality. This allowed detailed mapping of the thermal bar and water quality variations observed in the near shore of the thermal bar. The study showed that in general both HCMM's spatial and thermal resolution were adequate for large water resource studies.

### 1.4.3 Use of Regular IR Satellite Data to Investigate Thermal Bar and Upwelling Phenomenon (I. A. Bychkova and Demina, 1989)

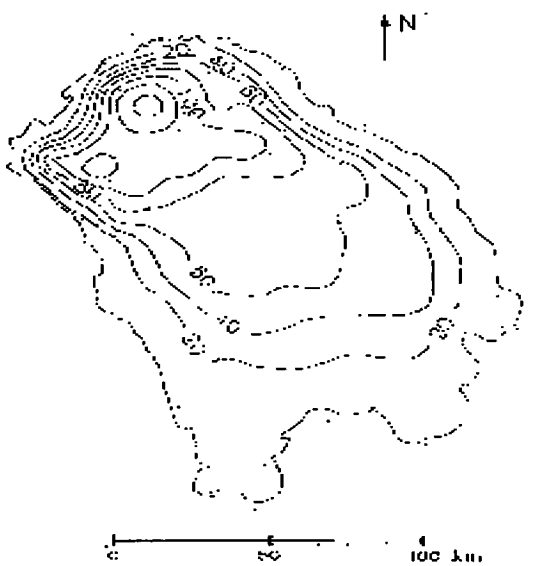


Figure 1.6: Bathymetric profile of Lake Ladoga (Malm and Jonsson, 1993)

The above study was conducted by (I. A. Bychkova and Demina, 1989) on Lake Ladoga in the Spring and Summer of 1986. IR satellite data obtained by AAPI, AtlantNIRO from $22^{nd}$ April to $8^{th}$ September along with the airborne ice survey by Szugks were used for the

above study. The movement of the thermal bar including the changes in the relative areas of the Thermally Inert (TI) and Thermally Active (TA) zones were reported to be visible in the satellite imagery. A linear regression equation obtained from the satellite data indicated the change in area of the TI zone $S(km^2)$ over time t(days) after the onset of hydrologic Spring (5 May 1996) to be

$$S = -280t + 19000$$

The estimate of S is considerably affected by diurnal variation in the surface temperatures according to satellite data. It was also observed that the area of the TI zone in the morning hours is considerably greater than evening. Therefore, when determining S (t) it is described to use information obtained at the same time of the day. Movement of the thermal bar averaged over the perimeter was observed to be constant at about $1\frac{km}{day}$ over prolonged periods. The actual speed of the movemen of the bar differed in the Southern and Northern parts of the lake owning to the great difference in the slope.

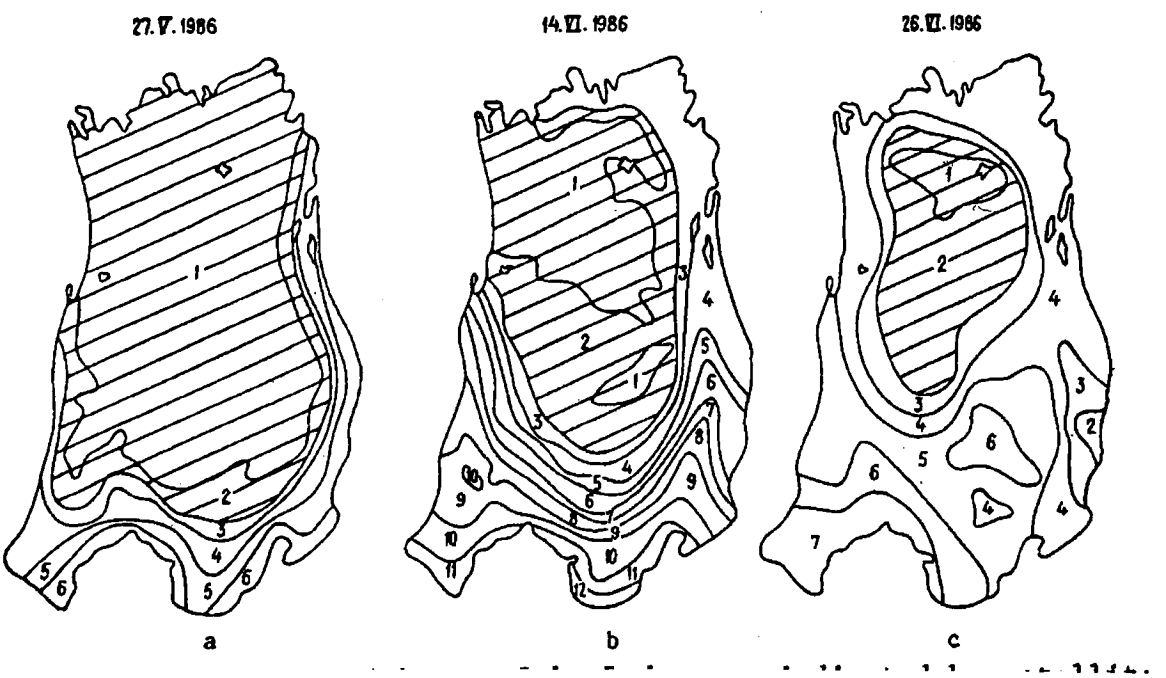


Figure 1.7: Movement of the Thermal bar on Lake Ladoga as indicated by satellite IR data

It is stated that at present it is difficult to observe the stripe of the thermal bar whose temperature is constant at $4^oC$ due to the rather low spatial resolution of the satellite radiometer. The upwelling or vertical water movement which causes deep water to emerge at the surface was observed in the above study. The upwelling temporal scale was found to range from $10-20$ minutes to $2-3$ days while the spatial distribution resolution on the lake surface ranged from hundreds of square meters to hundreds of square kilometers. However, satellites can observe only the largest upwelling areas. The upwelling zone detected by satellite data varied from $100km^2$ on $5^{th}$ August to $1500km^2$ on $7^{th}$ August 1986. In the Spring and Summer seasons of 1986, upwelling detectable in satellite data occurred once a month with areas of $100 - 1500km^2$, temperature differences of $2 - 6^oC$ and durations of about 4 days. It is concluded that satellite IR data can be used to observe the development of upwelling on Lake Ladoga. It is suggested that combination of satellite data with hydrometeorological data from weather stations would enable us to predict when the thermocline will reach the water surface from its rate of vertical ascent. These predictions can be made $1 - 3$ days in advance. Prediction of upwelling makes it possible to conduct controllable experiments in which buoy stations are emplaced in the zones with the greatest temperature gradients so that full information on the upwelling as a synoptic phenomenon could be observed and characterized. Because such a correlation exists between the position of the thermal bar and the depth contour, it could be assumed that the wind-induced currents are of minor importance as to the dynamics of the thermal bar (Malm and Jonsson, 1993). It was also stated in (Malm and Jonsson, 1993) that the model output is sensitive to $Q(t)$(heat flux) and initial temperature T o at the beginning of the thermal bar generation. Since the model output is very sensitive to the heat flux and since Lake Ladoga is a large lake, it brings the problem of possible variations in spatial distribution of the heat flux. It was also stated in (Malm and Jonsson, 1993) that the higher the value of T o is, the faster the thermal bar progression will be. For instance, if $T_o = 0.5^oC$ the thermal bar progression

rate will be 12% higher. We should also keep in mind the fact that $T_o$ also could be spatially dependent.

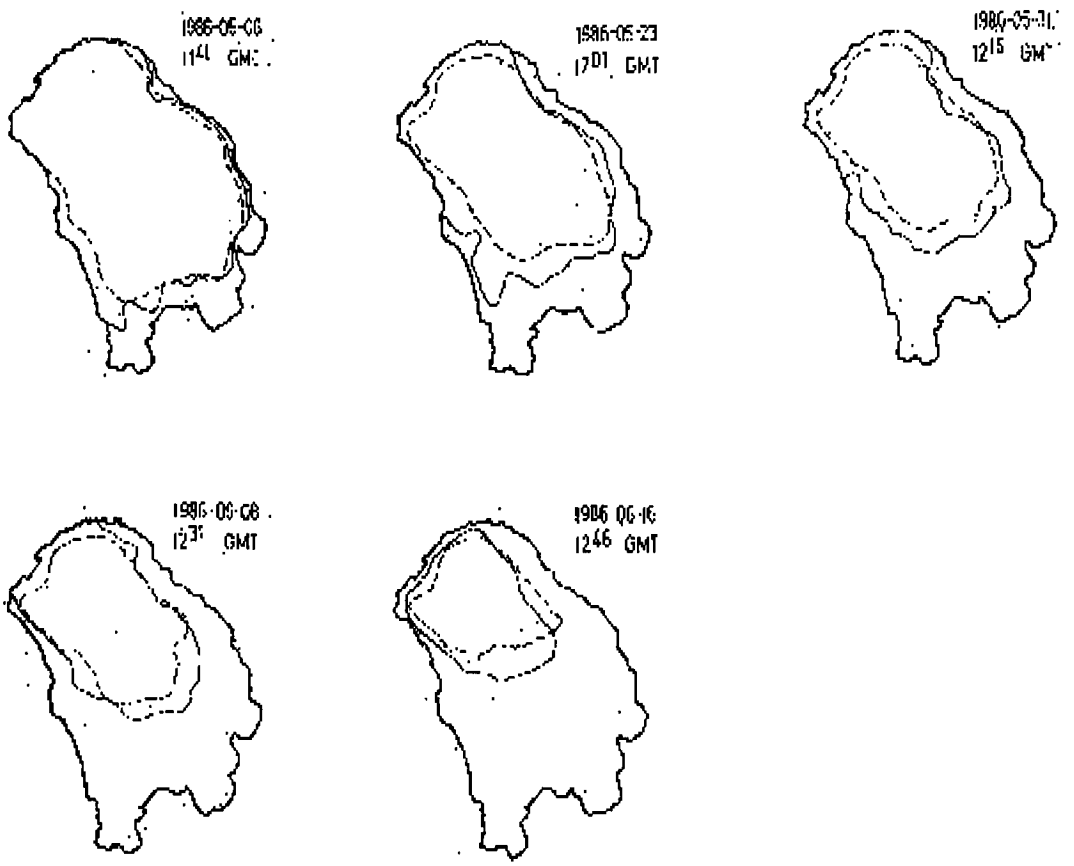


Figure 1.8: Propagation of the thermal bar on Lake Ladoga

### 1.4.4 Documentary Complex Surface Temperature Patterns from AVHRR Imagery of Sagniaw Bay.(J. W. Budd and Maclean, 1998)

(J. W. Budd and Maclean, 1998) at MTU have used AVHRR images to derive the surface temperature of the Saginaw bay. Saginaw bay is a large estuary that discharges into Lake

Huron, through a mouth that is $42km$ wide.The main objective of the study is to identify surface temperature patterns related to season and winds using AVHRR images in conjunction with meteorological data. The inner-bay is quite shallow (mean depth of $4.6m$) compared to the outer-bay ( mean depth of $15m$). Because of its shallow depth, the water volume of the inner bay is only 39% of the bay's total water volume. An additional feature includes a relatively deep channel that runs from the outer bay through the inner bay.

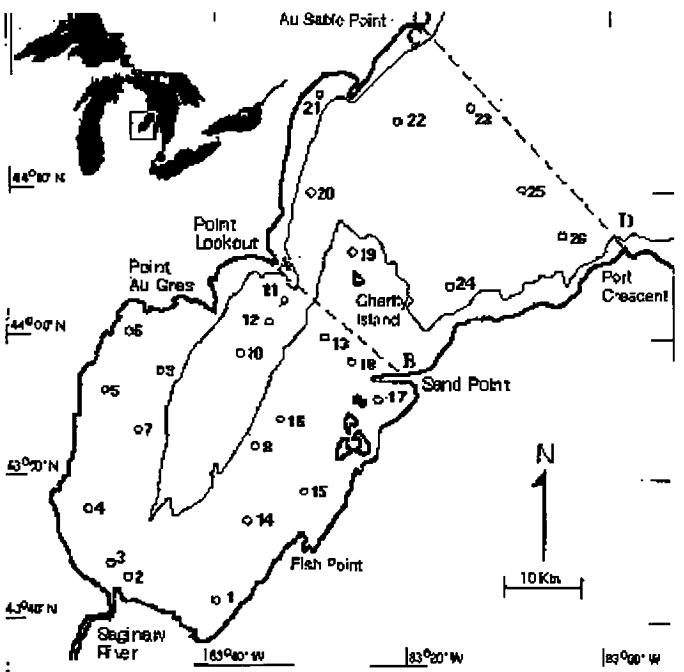


Figure 1.9: Location map of Sagniaw Bay, Lake Huron. NOAA/GLERL sampling locations are numbered 1 to 26

Wind stress and Lake Huron coastal currents interact to create highly variable circulation conditions within the bay. The outer bay circulation is characterized as counter-clockwise yet completely different current patterns could arise from changing wind characteristics, suggesting frequent internal mixing of inner bay waters. The studies conducted on Sagniaw bay show that outer bay circulation could also shift from clockwise to counter

clockwise implying complex mixing in these waters. Additional complication factors involve the Saginaw river discharge. Where as the outer bay is influenced by coastal currents, the inner bay is heavily influenced by occasionally large seasonal inputs from the Sagniaw river. As mentioned above many factors influence the circulation of waters within Saginaw bay and mixing with lake Huron. The AVHRR images that were used for the above study were obtained from the NOAA Coastal Active Access System (NCAAS). NCAAS is an archiving service provided through the NOAA Coast watch Program. The already geo-referenced images were converted to degrees Celsius using two of the three multi-channel sea Surface Temperature (MCSST) algorithms. 643 sampling days over the 3−year period from 1st April to $31^{st}$ October were used. The selection of cloud free images for Sagniaw bay was based on visual analysis of near infrared (Channel 2), aerosol-corrected reflectance (channel 1 minus channel 2). A freeware software called DECCON available through Coast Watch, was used to remove header information contained in the files and convert it to a format suitable for importing to an image processing software. Because of a clock error on the satellite the images were misregistered.

The Coast Watch program has implemented three sets of operational programs that accounts for the effects of the atmospheric water vapor. Only two of the three daytime algorithms were used to derive the temperature. The algorithms were namely IMGMAP and OCNMAP. Shipboard temperatures were collected by 26 sampling stations, within 1 to 10 hours of the satellite overpass. Eighteen of the sampling stations fell within the inner bay, whereas eight were in the outer bay. The images were registered to fit the bulk temperature stations. There was a very close approximation between the bulk temperature and the image derived temperature.

Comparison of the algorithms IMGMAP and OCNMAP intercepts and slopes indicated no significant differences between the regression coefficents. The above provided better estimates of bulk temperature in the mid-temperature ranges, from 15 to $25^{o}C$.

According to the study it was found that AVHRR imagery confirmed known seasonal thermal phenomena. A snapshot of six images from 1993 clearly documented the formation and the propagation of the thermal bar. Inter-annual variations were observed by comparing bulk temperature in 1991, 1992 and 1993. The onset of warming occurred several weeks earlier in 1991 and summer temperatures were an average of 5.6 and $3.4^oC$ higher in 1991 than 1992 and 1993.

### 1.4.5 Field investigation of the Thermal bar in Lake Ontario (Rodgers, 1971)

Field investigation of the thermal bar was conducted by (Rodgers, 1971), of the Great Lakes Institute of the University of Toronto in 1970. Twelve field surveys approximately two to three weeks apart, were conducted during the period early March to late June. The field collects were done along seven paths approximately parallel, with a spacing of about $25km$ apart to each other in the North-South direction between the longitude $77^o30^oW$ and $76^o30^oW$. The temperatures were collected about $3km$ apart on these parallel lines that are normal to the shoreline.

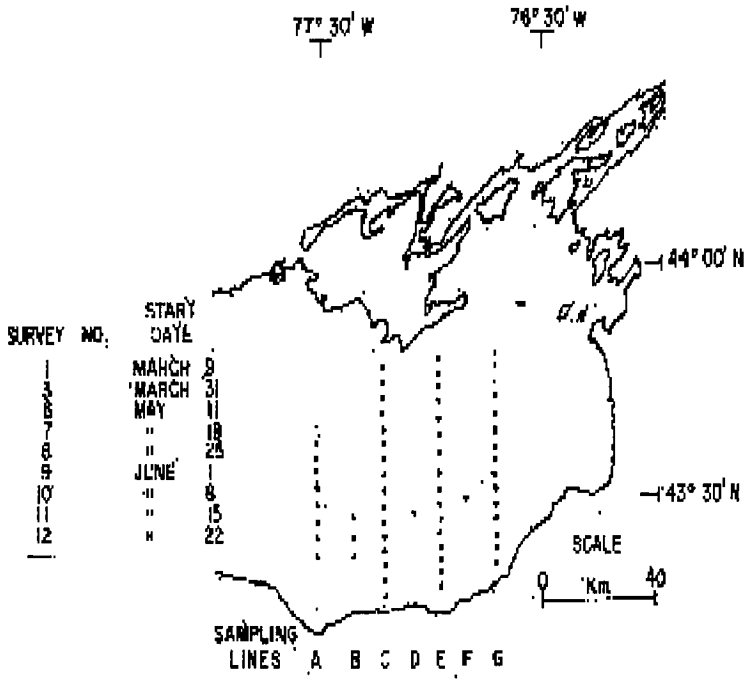


Figure 1.10: Field investigation of the Thermal bar in Lake Ontario : Sampling locations and survey dates

All vertical temperature profiles were reduced to averages over a ten-meter depth interval within each individual profile. The temperature was measured to a maximum depth of 200 meters.

### 1.4.6 Methods of Observation

Measurement of temperature profiles were carried out with mechanical bathythermographics with an accuracy of $\pm 0.2^oC$ and reversing thermometers with an accuracy of $\pm 0.02^oC$. Most of the observations were carried out with the standard mechanical bathythermograph with calibration done using reversing thermometers. The vertical temperatures were mea-

sured using a thermally uniform level where all sensors were within 10m of each other. Depth calibration was checked with a measured line to a maximum of $200m$. All temperature/depth data were reduced to average over a $10m$ depth interval within each individual profile.

### 1.4.7 Results and Analysis

The overall pattern of heat content change was identical to that observed by Rodgers 1968. The heat content change was calculated from the difference in temperature of the two temperature-depth measurements on the survey in a particular sampling region. When the thermal bar is close to the shore some small heat content changes were observed close to the shores. Higher than average heat content changes were observed between the positions of the thermal bar on the North side of the lake, but not on the South side. Very large positive heat content changes were observed in the middle of the lake during the last one to two weeks of the presence of the thermal bar associated with very small even negative changes in heat content along the North shore. It could be concluded that the differences in heat content change in the latter stages must be due to offshore advection of heat. It was also clearly observed that the speed of the thermal bar was inversely correlated with the lake bottom slope. Between surveys 6 and 10, the thermal bar moved with an average speed of $0.8cm/sec$ away from the North shore. The speed away from the South shore was $0.4cm/sec$. Substantial perturbations were observed in the general offshore progression of the bar. It was clear, given the temperature data for the flow along the bottom from the thermal bar to the deeper parts of the lake is extremely weak. The regions where the temperatures were less than $4^oC$ at the surface, where surface heating is taking place, appeared to be actively mixing to great depth. A close correlation was noticed between the observed positions of the thermal bar using the satellite data and the ones predicted by the model described earlier.

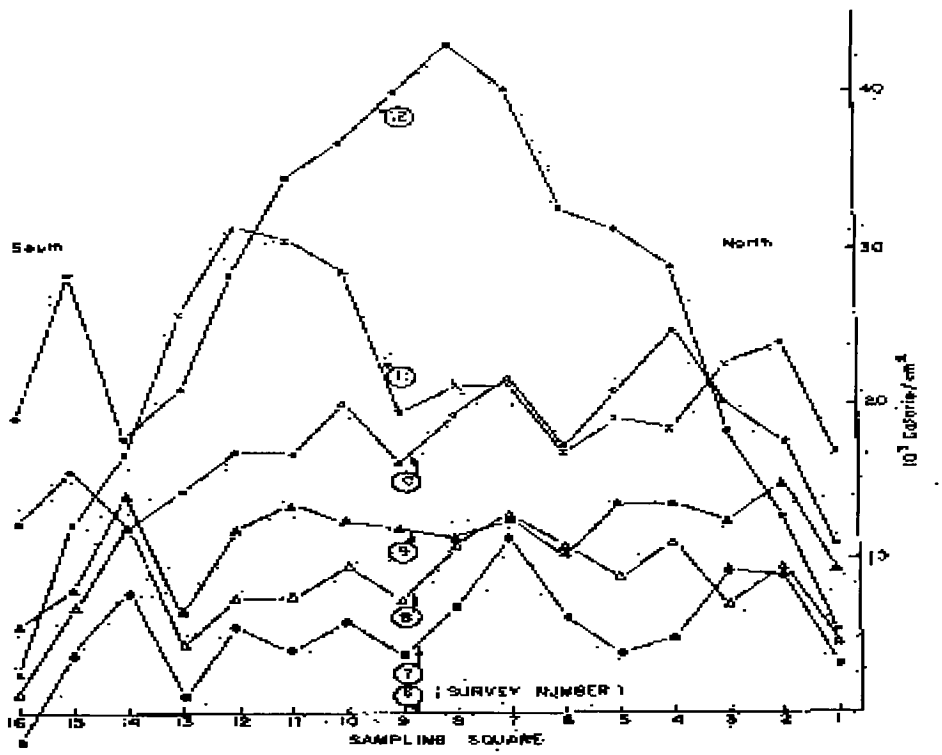


Figure 1.11: Heat content changes along Line C relative to surveys 1 to 12 March $9^{th}$ to June $22^{nd}$1970

(Rodgers, 1971)

# Chapter 2

# Theory

## 2.1 Sea Surface Temperature Measurements from Space

Infrared measurements have been used since 1970 to estimate sea surface temperature from space. Solutions are also required to practical problems such as correcting for the effects of the intervening atmosphere identifying cloud-free regions and navigating the measurements to ground coordinates (Monaldo, 1997). The National Oceanic and Atmospheric Administration has two satellites (NOAA-12 and NOAA-14) equipped with the Advanced Very Height Resolution Radiometer (AVHRR) which has a nadir resolution of 1.1km and twice-daily global coverage.

### 2.1.1 Blackbody Radiation

By virtue of molecular motion, all substances above absolute zero emit and absorb specific quantities of radiation. A blackbody is an idealization surface or cavity that has the property that all incident electromagnetic flux is perfectly absorbed and then re-radiated (i.e. the reflection is zero and absorbivity is one) (Schott, 1997). Wien derived a simple expression for the wavelength distribution of the radiation from a black body ($B(\lambda, T)$) to be

$$B(\lambda, T) = \frac{f(\lambda T)}{\lambda^5}$$

Where T is the absolute Temperature and $f(\lambda T)$ is a function of the product of wavelength and temperature.

In 1901 Plank made the simple assumption that energy can only exist in discrete packets or quanta. The energy in a quanta was defined to be equal to $h\nu$ where $h$ is the Planck's constant and $\nu$ is the electromagnetic frequency. Planck used the above to derive an expression for vibrational energy states between atoms. With the assumption that the vibrational resonation between the atoms could only emit or absorb energy in discrete levels propotional to the frequency of the oscillation state. Hence the energy states are defined by $Q = mh\nu$ where $m$ is an integer value.

Further from this and thermodynamic considerations, Planck derived the blackbody radiation equation for the special radiant exitance from a surface as

$$M_\lambda = 2\Pi hc^2\lambda^{-5}(e^{\frac{hc}{\lambda kT}} - 1)^{-1}[Wm^2\mu m^{-1} \tag{2.1}$$

where $T$ is the absolute temperature, $k$ is the Boltzmann gas constant and $c$ is the speed of light. By holding the temperature fixed at selected values a family of backbody curves can be generated, relating spectral exitance to wavelength (Schott, 1997).

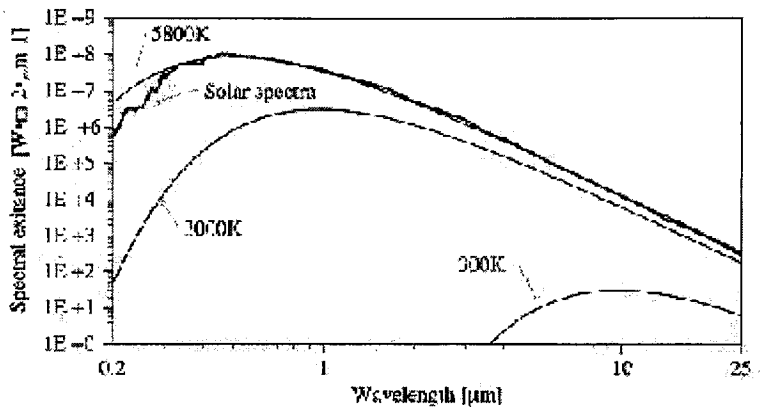


Figure 2.1: Blackbody curves and solar exitance spectra (Schott, 1997) page 61

### 2.1.2 Estimation of Temperature

For any observed radiation measured at a specific wavelength there is an associated temperature such that at that temperature a blackbody would emit the same radiation. In other words, it we know the emissivity of a body and measure the emitted radiance, then we can determine the body's true surface temperature. Emissivity $\varepsilon(\lambda)$ is defined as the ratio of the spectral existence from a target $M_\lambda(T)$ to that from a blackbody at that temperature $M_{\lambda BB}(T)$

$$\varepsilon(\lambda) = \frac{M_\lambda(T)}{M_{\lambda BB(T)}} \tag{2.2}$$

(Schott, 1997) The emissivity describes how well an object radiates energy compared to the perfect black-body radiator and is a fundamental property of matter. There are several limitations to using radiance measurements from a space-borne platform. The main limitation is the clouds : clouds block infrared radiation. Therefore the clouds have to be appropriately identified and masked out. Also the atmosphere attenuates some of the radiation emitted from the surface. Therefore predefined methods/algorithms should be used to correct the radiance due to all the above. There is also the factor contributed by the Solar radiance that is reflected from the object directly to the sensor, which has to be detected and removed.

### 2.1.3 Sea Surface Temperature Algorithms

**Functional Form of the Sea Surface Temperature Algorithm (Monaldo, 1997)**

Let $N(T)$ represent the blackbody radiance at temperature T in a specified wavelength regime. The radiance measured at a satellite is the sum of the ocean radiance, plus radiance emitted from the atmosphere, plus the sky radiance reflected from the surface.

$$N_m(T_m) = \tau_a \varepsilon_w N(T_s) + \varepsilon_a N(T_a) + \tau_a r_w N_{sky} \tag{2.3}$$

$N_m(T_m)$: Measured radiance

$\tau_a \varepsilon_w N(T_s)$:Water surface

$\varepsilon_a N(T_a)$:Atmosphere

$\tau_a r_w N_{sky}$:Reflected Sky Radiance

$N_m$ : radiance measured at the satellite

$\tau_a$: is the transmittance of the atmosphere

$\varepsilon_w$: is the emissivity of water

$N(T_s)$: is the blackbody radiance at the sea surface temperature of $T_s$

$r_w$: is the reflectivity of water, and

$N_{sky}$: is the downwelling sky radiance

We know that atmospheric emissivity, $\varepsilon_a$, equals $(1 - r_a)$ and that the emissivity of water, $\varepsilon_w$ equals $(1 - r_w)$. We substitute these relations in equation (2.3)

$$N_m(T_m) = \tau_a \overbrace{(1 - r_w)} N(T_s) + \overbrace{(1 - r_a)} N(T_a) + \tau_a r_w N_{sky} \tag{2.4}$$

Rearranging terms yields

$$N_m(T_m) = \tau_a N(T_s) - r_w \tau a N(T_s) + N(T_a) - \tau_a N(T_a) + \tau_a r_w N_{sky} \tag{2.5}$$

or

$$N_m(T_m) = \tau_a N(T_s) - \overbrace{r_w \tau_a N(T_s) \left[1 - \frac{N_{sky}}{N(T_s)}\right]} + (1 - \tau_a) N(T_a) \tag{2.6}$$

Since the reflection coefficient indicated by $\overbrace{r_w \tau_a N(T_s) \left[1 - \frac{N_{sky}}{N(T_s)}\right]}$ of water is small, we eliminate the middle term on the right-hand side of the previous equation and get

$$N_m(T_m) = \tau_a N(T_s) + (1 - \tau_a) N(T_a) \tag{2.7}$$

We now perform a Taylor's series expansion for $N_m(T_m)$ about the sea surface temperature, keeping the first two terms. We rewrite $N_m(T_m)$ as

$$N_m(T_m) = N(T_s) + \frac{\partial N(T_s)}{\partial T}((T_m) - (T_s)) \tag{2.8}$$

Substitute this relation into the left-hand side of Equation 2.7. The resulting equation is

$$N(T_s) + \frac{\partial N(T_s)}{\partial T}(T_m - T_s) = \tau_a N(T_s) + (1 - \tau_a) N(T_a) \tag{2.9}$$

We may also expand $N(T_a)$ as

$$N_m(T_m) = N(T_s) + \frac{\partial N(T_s)}{\partial T}(T_a - T_s) \tag{2.10}$$

Substitution of this into equation 2.9 yields

$$N(T_s) + \frac{\partial N(T_s)}{\partial T}(T_m - T_s) = \tau_a N(T_s) + (1 - \tau_a) \left[N(T_s) + \frac{\partial N(T_s)}{\partial T}(T_a - T_s)\right] \tag{2.11}$$

By eliminating like terms in the previous equation and dividing by $\frac{\partial N(T_s)}{\partial T}$ we get

$$T_m = \tau_a T_s + (1 - \tau_a) T_a \tag{2.12}$$

Equation 2.12 is valid at two channels $i$ and $j$ and we can rewrite Equation 2.12 for two wavelengths as

$$T_i = \tau_{a_i} T_s + (1 - \tau_{a_i}) T_{a_i} \tag{2.13}$$

and

$$T_j = \tau_{a_j} T_s + (1 - \tau_{a_j}) T_{a_j} \tag{2.14}$$

The difference $T_i - T_j$ is then given as

$$T_i - T_j = T_s(\tau_{a_i} - \tau_{a_j}) + (1 - \tau_{a_i}) T_{a_i} - (1 - \tau_{a_j}) T_{a_j} \tag{2.15}$$

By multiplying Equation 2.13 by $\tau_{a_j}$ and Equation 2.14 by $\tau_{a_i}$, we generated the following two equations:

$$\tau_{a_j} T_i = \tau_{a_i} \tau_{a_j} T_s + (1 - \tau_{a_i}) T_{a_i} \tag{2.16}$$

$$\tau_{a_j} T_j = \tau_{a_i} \tau_{a_j} T_s + (1 - \tau_{a_j}) T_{a_j} \tag{2.17}$$

We now subtract equation 2.17 from equation 2.16, yielding

$$\tau_{a_j} T_i - \tau_{a_j} T_j = \tau_{a_j}(1 - \tau_{a_i}) T_{a_i} - \tau_{a_i}(1 - \tau_{a_j}) T_{a_j} \tag{2.18}$$

Subtracting equation 2.18 from equation 2.15, we write

$$\begin{aligned} T_i(1 - \tau_{a_j}) - T_j(1 - \tau_{a_i}) =& T_s(\tau_{a_i} - \tau_{a_j}) + \left[(1 - \tau_{a_i}) - \tau_{a_j}(1 - \tau_{a_i})\right] \\ & T_{a_i} - T_s(\tau_{a_i} - \tau_{a_j}) + \left[(1 - \tau_{a_j}) - \tau_{a_i}(1 - \tau_{a_j})\right] T_{a_j} \\ =& T_s(\tau_{a_i} - \tau_{a_j}) + (1 - \tau_{a_i})(1 - \tau_{a_j}) T_{a_i} - (1 - \tau_{a_j})(1 - \tau_{a_i}) T_{a_j} \end{aligned} \tag{2.19}$$

Subtracting for $T_s$ we obtained

$$T_s = T_i + \frac{1-\tau_{a_i}}{\tau_{a_i}-\tau_{a_j}}(T_i - T_j) - \frac{(1-\tau_{a_i})(1-\tau_{a_j})}{\tau_{a_i}-\tau_{a_j}}(T_{a_i} - T_{a_j}) \tag{2.20}$$

We conclude that the absence of clouds and observations at nadir, sea surface temperature may be written as

$$T_s = a_0 T_i + a_1(T_i - T_j) + a_2 \tag{2.21}$$

For the approximations used here, $a_0 = 1$, i.e., at the lowest order the sea surface temperature equals the measured brightness temperature.The parameter $a_1(T_i - T_j)$ accounts for the atmospheric transmittance. The last term is a small correction associated with the different brightness temperatures of the atmosphere at the two measurement wavelengths.

### Coefficients for Sea Surface Temperature Algorithms

In addition to equation 2.21, there are correction terms that must be applied to adjust the measurements made off nadir. If we define $\theta$ to be the sensor zenith angle, then the three algorithms have the form:

### Split window

$$T_s = A_0 T_{11} + A_1(T_{11} - T_{12}) + A_2(T_{11} - T_{12})(\sec\theta - 1) + A_3 \sec\theta + A_4 \tag{2.22}$$

In the above $T_{11}$ and $T_{12}$ are the digital counts obtained from bands 4 and 5 respectively.

| Satellite | Time | $A_0$ | $A_1$ | $A_2$ | $A_3$ | $A_4(K)$ |
|---|---|---|---|---|---|---|
| NOAA-14 | Day | 1.017342 | 2.139588 | 0.779706 | 0.000 | -5.280 |
| NOAA-14 | Night | 1.029088 | 2.275385 | 0.752567 | 0.000 | -9.090 |
| NOAA-12 | Day | 1.013674 | 2.443474 | 0.314312 | 0.000 | -4.647 |
| NOAA-12 | Night | 1.013674 | 2.443474 | 0.314312 | 0.000 | -4.647 |

**Dual window**

$$T_s = A_0 T_{11} + A_1(T_{3.7} - T_{11}) + A_2(T_{3.7} - T_{11})(\sec\theta - 1) + A_3 \sec\theta + A_4 \tag{2.23}$$

In the above $T_{3.7}$ and $T_{11}$ are the digital counts obtained from bands 3 and 4 respectively.

| Satellite | Time | $A_0$ | $A_1$ | $A_2$ | $A_3$ | $A_4(K)$ |
|---|---|---|---|---|---|---|
| NOAA-14 | Night | 1.008751 | 1.409936 | 0.000000 | 1.976 | -0.764 |
| NOAA-12 | Day | 1.017736 | 0.426593 | 1.800916 | 0.0 | -3.114 |
| NOAA-12 | Night | 1.017736 | 0.426593 | 1.800916 | 0.0 | -3.114 |

## 2.2 ALGE- The 3D Hydrodynamic Model (Garrett, 1997)

### 2.2.1 Hydrodynamic Equations

ALGE is a 3D Hydrodynamic model that was developed at the Department of Energy. The equations used in ALGE are very similar to those used by most researchers to predict the behavior of bodies of water with a free surface. ALGE uses carteasian coordinates in the horizontal and vertical planes. It solves the following standard set of hydrostatic equations.

$$\frac{\partial u}{\partial t} = -\frac{\partial uu}{\partial x} - \frac{\partial vu}{\partial y} - \frac{\partial wu}{\partial z} - \frac{1}{\rho}\frac{\partial p}{\partial x} + f_v + \frac{\partial\left(K_H \frac{\partial u}{\partial x}\right)}{\partial x} + \frac{\partial\left(K_H \frac{\partial u}{\partial y}\right)}{\partial y} + \frac{\partial\left(K_Z \frac{\partial u}{\partial z}\right)}{\partial z} \quad (2.24)$$

$$\frac{\partial v}{\partial t} = -\frac{\partial uv}{\partial x} - \frac{\partial vv}{\partial y} - \frac{\partial wv}{\partial z} - \frac{1}{\rho}\frac{\partial p}{\partial y} - f_u + \frac{\partial\left(K_H \frac{\partial v}{\partial x}\right)}{\partial x} + \frac{\partial\left(K_H \frac{\partial v}{\partial y}\right)}{\partial y} + \frac{\partial\left(K_Z \frac{\partial v}{\partial z}\right)}{\partial z} \quad (2.25)$$

$$\frac{\partial T}{\partial t} = -\frac{\partial uT}{\partial x} - \frac{\partial vT}{\partial y} - \frac{\partial wT}{\partial z} + \frac{\partial\left(K_H \frac{\partial T}{\partial x}\right)}{\partial x} + \frac{\partial\left(K_H \frac{\partial T}{\partial y}\right)}{\partial y} + \frac{\partial\left(K_Z \frac{\partial T}{\partial z}\right)}{\partial z} \quad (2.26)$$

$$\frac{\partial w}{\partial z} = -\frac{\partial u}{\partial x} - \frac{v}{y} \quad (2.27)$$

$$\frac{\partial p}{\partial z} = -\rho g \quad (2.28)$$

$u$,$v$ and $w$ are velocity components, $T$ is temperature, $K_H$ and $K_Z$ are the horizontal and vertical diffusion coefficients, $f$ is the Coriolis parameter, $g$ is the gravitational acceleration, $P$ is the hydrostatic pressure and $\rho$ is the density of water. Alogarithmic relationship is used to model bottom drag at the lower level of the model. ALGE treates the energy losses to the atmosphere separately.

Density ($kg/m^3$) is related to temperature ($^oC$) by a quadratic equation given by

$$\rho = 0.99987 + 6.6724x10^{-5} - 8.8191x10^{-6}T^2 + 7.9953x10^{-8}T^3 - 5.7701x10^{-10}T^4 + 1.7549x10^{-12}T^5$$

Vertically integrated versions of 2.24, 2.25 and 2.27 are also solved to produce time-varying free surface elevations for use in computation of pressure gradients in 2.24, 2.25 and

pressure in 2.28. The vertically integrated forms of 2.24, 2.25and 2.27 are derived by first introducing a transformed, terrain-following vertical coordinates.

$$z^{\star} = z - z_g(x, y)$$

Where $z_g$ is the lake bottom elevation relative to an arbitrary reference height. The above produces the following equations.

$$\frac{\partial Uh}{\partial t} = -\frac{\partial U^2 h}{\partial x} - \frac{\partial UVh}{\partial y} + h\frac{\partial\left(K_H \frac{\partial U}{\partial x}\right)}{\partial x} + h\frac{\partial\left(K_H \frac{\partial U}{\partial y}\right)}{\partial y} + fV_h - g\left(h\frac{\partial h}{\partial x} + h\frac{\partial z_g}{\partial x}\right) - C_D(U^2+V^2)^{\frac{1}{2}}U + C_s\rho_a W^2\frac{\cos\psi}{\rho_o} \tag{2.29}$$

$$\frac{\partial Vh}{\partial t} = -\frac{\partial V^2 h}{\partial y} - \frac{\partial UVh}{\partial x} + h\frac{\partial\left(K_H \frac{\partial V}{\partial x}\right)}{\partial x} + h\frac{\partial\left(K_H \frac{\partial V}{\partial y}\right)}{\partial y} - fU_h - g\left(h\frac{\partial h}{\partial y} + h\frac{\partial z_g}{\partial y}\right) - C_D(U^2+V^2)^{\frac{1}{2}}V + C_s\rho_a W^2\frac{\sin\psi}{\rho_o} \tag{2.30}$$

$$\frac{\partial h}{\partial t} = -\frac{\partial Uh}{\partial x} - \frac{\partial Vh}{\partial h} + M_s \tag{2.31}$$

$U$ and $V$ are vertically integrated horizontal velocity components; $h$ :water depth; $\rho_o$ :reference density ($1g/cm^3$); $C_D$ : bottom drag coefficient; $C_s$ : air-water surface drag coefficient; $\rho_a$ :air density; $W$ : wind speed; $\psi$ : angle of the x-axis from the North; and $M_s$ : mass source or sink. The drag coefficient is related is related to the roughness length by the logarithmic law

$$C_D = k^2[\ln(0.5\frac{\Delta z}{z_0})]^{-2}$$

where

$k$ : Von Karman's constant (0.4)
$z_o$ : roughness length
$\Delta z$ : vertical grid spacing

The roughness length is user specified and was set to $0.001m$ for all simulations.

### 2.2.2 Mixing Parameterizations

The horizontal eddy viscosities are diffusivities ($K_H$) are primarily based on a version of the Smagorinsky (1963) model.

$$K_S = C_{Sh}\Delta^2 S$$

where

$$C_{Sh} = 0.02$$

;

$$\Delta = (\Delta x \Delta y)^{0.5}$$

and

$$S = (S_{ij}S_{ij})^{\frac{1}{2}}$$

where S is a scalar function of the large scale strain rate tensor, i.e.

$$S_{ij} = \frac{1}{2}\left[\frac{\partial U_i}{\partial x_j} + \frac{\partial U_i}{\partial x_i}\right]$$

The scheme used to compute vertical eddy diffusivity in this research combines elements of methods presented by (Yamada, 1983) and (Garrett, 1983). Both of these methods are simplified versions the level 2.5 turbulence model developed by (Mellor and Yamada, 1982). A prognostic equation is solved for the turbulent kinetic energy

$$\begin{aligned}\frac{\partial E}{\partial t} = &- \frac{\partial uE}{\partial x} - \frac{\partial vE}{\partial y} - \frac{\partial wE}{\partial z} + \frac{\partial\left(K_H \frac{\partial E}{\partial x}\right)}{\partial x} + \frac{\partial\left(K_H \frac{\partial E}{\partial y}\right)}{\partial y} + \frac{\partial\left(K_Z \frac{\partial E}{\partial z}\right)}{\partial z} - \\ &K_Z\left[\left(\frac{\partial u}{\partial z}\right)^2 + \left(\frac{\partial v}{\partial z}\right)^2\right] + g\alpha_T K_Z \frac{\partial T}{\partial z} - \frac{(2E)^{1.5}}{c_3 l}\end{aligned} \tag{2.32}$$

where E = turbulent kinetic energy; $\alpha_T$= coefficient of thermal expansion for water; $c_3$ = a constant (16.6); and $l$ = turbulent length scale defined by

$$l = min(\Delta z, l_z)$$

where $\Delta z$ =verical grid spacing and $l_z$ =turbulent length scale for stably stratified conditions $l_z = 0.76\frac{E^{0.5}}{\omega_b}$ and $\omega_b$ is the Brunt-Vaisala frequency. The vertical eddy diffusivity is defined as

$$K_z = l(2E)^{0.5} S_m$$

$S_m$ is an algebraic function defined by(Yamada, 1983) that accounts for the effects of stable density stratification on turbulence.

### 2.2.3 Energy Transfer

Exchange of energy between the surface layer of a body of water modelled by ALGE and the atmosphere is computed separately from the advection and diffusion computations.

$$\frac{dT}{dt} = (H_s + H_L + S_W + L_W)/(\triangle Z_S \rho_w c_{pw}) \tag{2.33}$$

where $H_S$ is sensible heat flux, $H_L$ is latent heat flux, $S_W$ is solar radiation, $L_W$ is thermal radiation, $\triangle Z_S$ is surface layer depth, $\rho_W$ is water density and $c_{pw}$ is specific heat of water.

#### Sensible and Latent Heat Transfer

The fluxes can be written as

$$H_S = a^2 W \triangle \theta F \rho_a C_p \tag{2.34}$$

and

$$H_L = a^2 W \triangle q F \rho_a L \tag{2.35}$$

$R$ : 0.74
$\rho_a$ : air density
$C_p$ : specific heat of air
$L$ : latent heat of evaporation
$F$ : flux profile parameterization using $R_i$
$\triangle q$ : specific humidity difference across surface layer

$$a^2 = \frac{k^2}{[\ln(\frac{z}{z_o})]}^2 \tag{2.36}$$

$k$ : von Karman's constant (0.4)
$z_o$ : roughness length over water (0.0002 m)

The flux profile parameterization F is defined by

$$F = 1 - \frac{bR_i}{1 + C\sqrt{|R_i|}} \tag{2.37}$$

for $R_i < 0$ and

$$F = (1 + \frac{bR_i}{2})^{-2}$$

for $R_i > 0$, and where $b = 9.4$ and $C = 5.3a^2\sqrt{\frac{z}{z_o}}$

**Shortwave (Solar) Radiation**

The direct and the diffuse solar radiation reaching the ground is computed from.

$$F = S_o(\tau_d \tau_{ws}^w \tau_{wa}^w)^M \cos\zeta \tag{2.38}$$

$\tau_d, \tau_{ws}^w, \tau_{wa}^w$ are transmission functions which parameterize the effects of dry air scattering, water vapor scattering and vapor absorption respectively. The exponent w is total atmospheric water vapor content expressed as an equivalent water depth(cm), and M is a pressure-adjusted optical depth. The coefficients $S_o$ is the normal solar flux above the troposphere and $\zeta$ is the zenith angle. The pressure-adjusted optical depth M is defined by $M = \frac{mp}{P_o}$, where m is the optical depth, p is atmospheric pressure at the location of interest and $P_o$ is sea level pressure($1013mb$). The optical depth is defined by $m = sec\zeta$ for $\zeta < 70^o$

$$m = \frac{[-R\cos\zeta + (R^2\cos^2\zeta + 2RH_S + H_S^2)^{0.5}]}{H_S} \tag{2.39}$$

for $\zeta > 70^o$. Also, R is the radius of the earth and $H_S$ is an atmospheric scale height(10km). The transmission functions and $S_o$ are defined by

$$\tau_d = 0.9 + 0.01(-0.1m^2 + 1.3m - 0.6)$$

$$\tau_{WZ} = 0.975$$

$$\tau_{WA} = 1 - \frac{0.19685}{[1 + \frac{1}{0.6992\sqrt{mw}}]}$$

$$S_o = 0.98 S_c (\frac{\phi_m}{\phi})^2$$

$S_C$ is the solar constant $(1.94 cal/cm^2/s)$, $\phi_m$ is the mean earth to sun distance of $1.49x10^8 km$, and $\phi$ is the actual distance, which is a function of the Julian day(J).

$$\phi = 149 - 2.6 sin(\frac{\pi}{2} - \frac{J\pi}{182.5}) \tag{2.40}$$

When clouds are present, transmission functions must be used to deplete the solar flux. Cumulus and stratocumulus are usually the dominant depleters of solar radiation. Transmission functions for these cloud typed are.

$$\tau_{cw} = 0.17 - 0.21 \cos\zeta$$

$$\tau_{st} = 0.28 - 0.16 \cos\zeta$$

for $\zeta < 0.2$, and

$$\tau_{cu} = 0.10 + 0.14 \cos\zeta$$

$$\tau_{st} = 0.19 + 0.28 \cos\zeta$$

for $\cos\zeta > 0.2$ The net surface global radiation is

$$S_W = (1 - A)(1 - \sigma_c + \sigma_c \tau) F$$

Where A is albedo of water, $\sigma_c$ is the amount of cloud cover($0 < \sigma_c < 1$), and $\tau$ is the cloud transmission function. The albedo (A) is computed

$$A = 0.5 \left[ \frac{\sin^2(i-r)}{\sin^2(i+r)} + \frac{\tan^2(i-r)\cos^2(i+r)}{\sin^2(i+r)} \right] \tag{2.41}$$

where r is the angle of reflection and $i$ is the angle of incidence, which are related through $n$, the refractive index $n = 1.33$

$$\sin(r) = \frac{\sin(i)}{n}$$

**Longwave Radiation**

The net surface longwave radiative flux is computed with simplified transmission model that treats emission and absorption in combined spectral bands. Clouds are treated as blackbodies and emission and absorption above the tropopause is neglected. The general case of partly cloudy skies is treated. The flux contributed by a spectral group $j$ is computed from.

$$\begin{aligned} L_{wf} =& \sigma_{sb}(T_S^4 - T_l^4) + p_j \sum_{i=1}^{I_C} \frac{\phi_i(e^{-k_j w_{i+1}})}{k_j} + \\ & (1-\sigma_c)[\frac{\phi_i p_j \sum_{i=I_{e+1}^{lr}}^{I_C}(e^{-k_j w_{i+1}})}{k_j}] + p_j e^{-k_j w_i} B(T_i) \end{aligned} \tag{2.42}$$

where

$$\phi_i = \frac{B(w_{i+1} - B(w_i))}{w_{i+1} - w_i}$$

and

$$L_w = \sum_{j=1}^{J} L_{wj}$$

The variables for the longwave radiation equations are defined below:

$\sigma_{sb}$ : Stefan-Boltzmann constant
$T_S$ : water surface temperature(K)
$T_1$ : surface layer air temperature (typically 10m)
$P_j$ : weighting coefficent
$k_j$ : absorption coefficient
$w$ : atmospheric equivalent water depth(cm)
$\sigma_c$ : cloud cover
$B$ : blackbody flux
$i$ : computational level
$I_C$ : cloud level(km)
$I_T$ : tropopause level.

The absorption and weighting coefficents are:

$$p_1 = 0.25$$

$$p_2 = 0.11$$

$$k_1 = 0.166$$

$$k_2 = 0.8$$

### 2.2.4 Boundary Conditions

There are three different options in the boundary conditions. The user could set the boundary such that

- The boundary would have a zero-gradient for temperature and the normal velocity component that is directed inward from the boundary.
- Keep the temperature and velocity fixed at the boundary
- zero-gradient boundary conditions for temperature and velocity throughout

### 2.2.5 Land-Water Distribution

ALGE uses a $2-D$ array to identify nodes that represent land ($0's$) and nodes that represent water ($1's$). ALGE assumes that all non-zero numbers are water. Special locations over water are

- mass and energy sources
- mass and energy sinks
- inflow and outflow boundaries

### 2.2.6 Surface Meteorological Data

ALGE uses hourly surface meteorological data. The variables included in the above are wind direction ($deg$), wind speed ($m/s$), temperature ($K$), dewpoint temperature ($K$), cloud cover ($0.0to1.0$), cloud height ($km$) and pressure ($mb$).

#### Preparation of Meteorological Data

Hourly metdata were down loaded from the following web-site $http://www.nndc.noaa.gov/cgi\text{-}bin/nndc/buyOL-002.cgi$. The above web-site has the speed in knots, temperature in Fahrenheit, pressure in Dynes. The data were down loaded and several utility programs were used to convert the data to the format ALGE recognizes.

Firstly the 'date' item was extracted to check for missing dates. For the missing dates, the data from the very closest dates before and after were extracted and interpolated for the missing dates. Then the interpolated data were substituted in-place of the missing dates.

Secondly the 'hour' column from the met-data was extracted and checked manually for any unexpected errors like invalid hours.

Once the above was done for each 'day' and the 'hour' column the data columns (wind speed, direction, temperature etc.) were extracted and interpolated for exact hourly values. Then the data were converted to the required formats.

### 2.2.7 Upper Air Meteorological data

ALGE uses hourly air data at specific heights above the lake surface. The only form of upper air meteorological data available is radio-sonde data taken twice a day at several heights.

#### Preparation of upper air Meteorological data

Firstly the heights with missing data values were extracted. Then the 'date' field was extracted and manually checked for missing dates. No replacement for the missing values were substituted at this stage.

The height, the pressure and the temperature were extracted from the file during the available days at $0hrs$ GMT and $12hrs$ GMT.

Then pressure and temperature were obtained by interpolation at specific heights of $100m$ above the surface and thereafter every $1km$ upto $10km$ above the surface. Once the above was done the temperature and the pressure at each height was used to calculate the water vapor at each of the above levels. Once the temperature and the water vapor were calculated at the specific heights at $0GMT$ and $12GMT$, the above two items were interpolated to obtain hourly water vapor and temperature values.

### 2.2.8 Tidal Forcing

The tidal forcing controls ALGE's estuarine simulations. In order to simulate flows driven by tidal forcing, time dependent water surface heights must be provided as an input file to ALGE. The National Oceanic and Atmospheric Administration (NOAA) provides Tidal Tables and Tidal Current Tables for many locations throughout the world.

As the variation in tidal forcing is periodic it could be modeled by a sin functions such as

$$h_B(t) - h_m = A\sin(C_t t_p)$$

where $A$ is the tidal amplitudes (one-half of the range) $h_B$ is the depth at the boundary, $h_m$ is the mean water depth, $t_p$ is a time variable and $C_t$ is defined as $C_t = \frac{\Pi}{P}$. where $P$ is half a semi-diurnal period ($P \sim 6hours$). Therefore according to the appropriate locations on Earth ALGE had to be given the above amplitudes and periods.

### 2.2.9 Water Depths

Water depths are read to ALGE via a file called idepth.dat. The depth at any location is represented by a number. The depths were obtained using a GIS database on the Great lakes. The GIS was created by using depth profiles obtained at several locations throughout the lake. These depth profiles were interpolated such that it forms a grided profile. Then the grided profile is used to create the idepth.dat file.

### 2.2.10 Other Input Parameters

The other input parameters that are needed are resolution of the bathymetric data, starting time (in Julian days), total simulation time, latitude, longitude, bottom roughness length, boundary inflow and outflow temperatures, mass sources temperature, mass source and sink flow rates, angle of x-axis from North, print interval, flags for time and parameter usage.

# Chapter 3

# Approach and Results

## 3.1 Case Studies on ALGE

### 3.1.1 Case studies with square Lakes

A bathymetry profile of a square lake was created, hourly weather data and radiosonde data were integrated for 90 days. The weather files and the radiosonde data were obtained from the Department of Energy for the case studies. The dimensions of the square lake were15 by 9 with horizontal and vertical resolution of $4km$ and $10m$ respectively.

Several case studies were conducted by varying the initial conditions of the lake. Specially, by varying the initial conditions and comparing it with the laboratory experiments conducted by Elliot & Elliot in 1969&1970. The thermal bar phenomenon has been studied in a quantitative manner using laboratory models. Studies have been conducted by variation of heat input, bottom slope and initial temperature to see the variations on the propagational speed of the thermal bar. A detailed descriptions of the Laboratory experiments were discussed in a previous chapter.

The results of the above laboratory studies indicated that the propagation of the thermal bar is rather sensitive to the initial temperature less than 4 degrees Celsius. The higher the value the higher the propagation of the thermal bar. This fact was clearly seen in the above case studies when the initial temperature were varied from $1.5^oC$ to $3.5^oC$ and it was clearly seen that as the initial temperature increased the propagational speed of the thermal bar. Which caused the thermal bar to form and disappear sooner. Since the results were according to the published laboratory experiments it was decided to continue case studies with more complex bathymetry.

### 3.1.2 Case studies on a false bathymetric lake

Two bathymetric profiles of the lake in the shape of Lake Ontario were created. One profile was similar to the depth profile of Lake Ontario, while the other was a shallower lake with largest depth equivalent to half of the maximum depth of Lake Ontario. Case Studies were

conducted similar to the case studies on the square lake by changing the initial conditions. The initial conditions that were changed were, the mean temperature of the lake during winter stratification, the cloud cover (varying - the solar energy onto the lake) and the wind speed. The above were varied to observe how it would effect the formation and the propagation of the thermal bar.

### 3.1.3 Methods of Analysis

At each of the above case studies the temperature of the surface was plotted. Also several positions on the lake were chosen and the temperature variation of that position with time was plotted. Which would give an important observation as to how each of the initial conditions including the different weather conditions effect the surface temperature of the lake spatially as well as temporally.

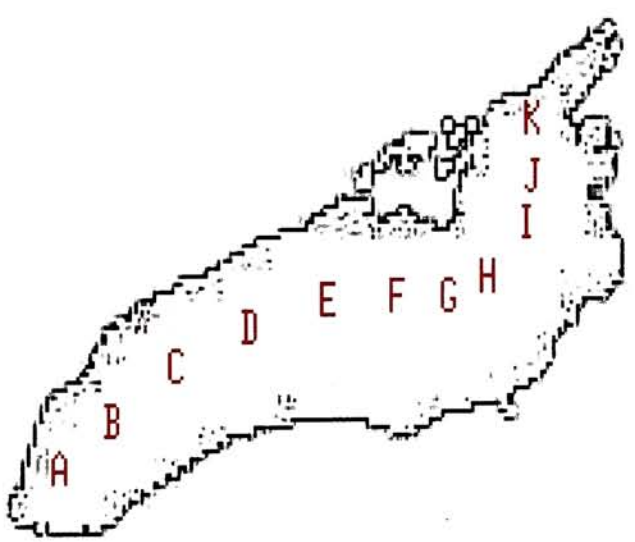


Figure 3.1: Methods of Analysis :Pixel positions


Figure 3.2: Methods of Analysis : color coding; The colour spectrum shows the ascending order of the pixels from A to K

### 3.1.4 Case Study 1 : Changing the mean temperature of the lake during winter stratification

The temperature was varied from $1^oC$ to $3.5^oC$ in $0.5^0C$ steps and the variation of the surface profile was observed. The above methods of analysis were used to observe the impact on the lake by varying the mean temperature of the lake during winter stratification.

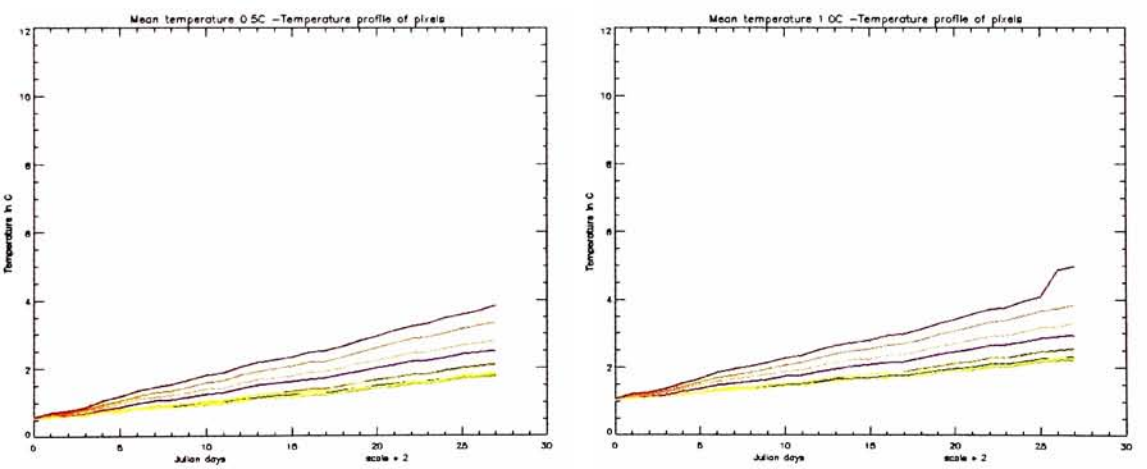


a) b)

Figure 3.3: Mean temperature of the lake during winter stratification image a)= $0.5^oC$; image b)= $1^oC$

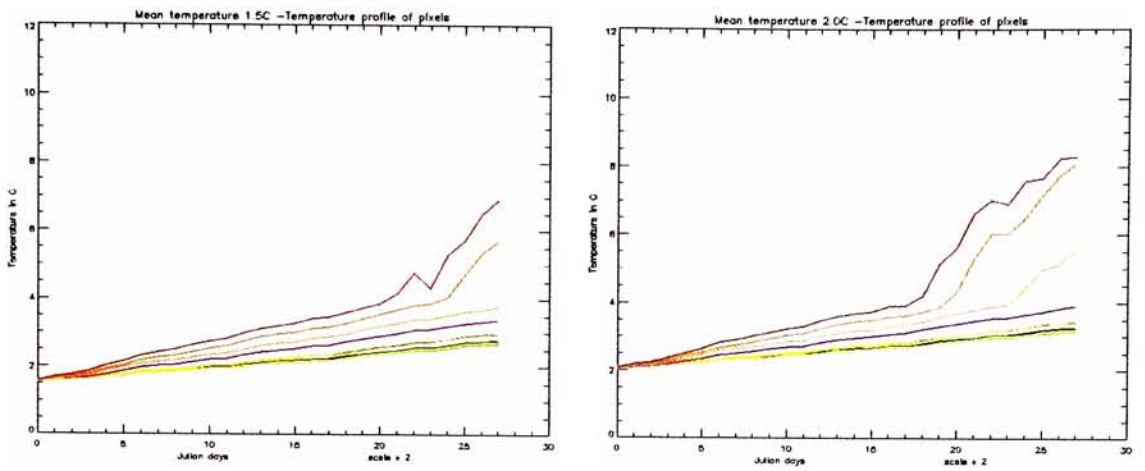


c) d)

Figure 3.4: Mean temperature of the lake during winter stratification image c)= $1.5^oC$; image d)= $2^oC$

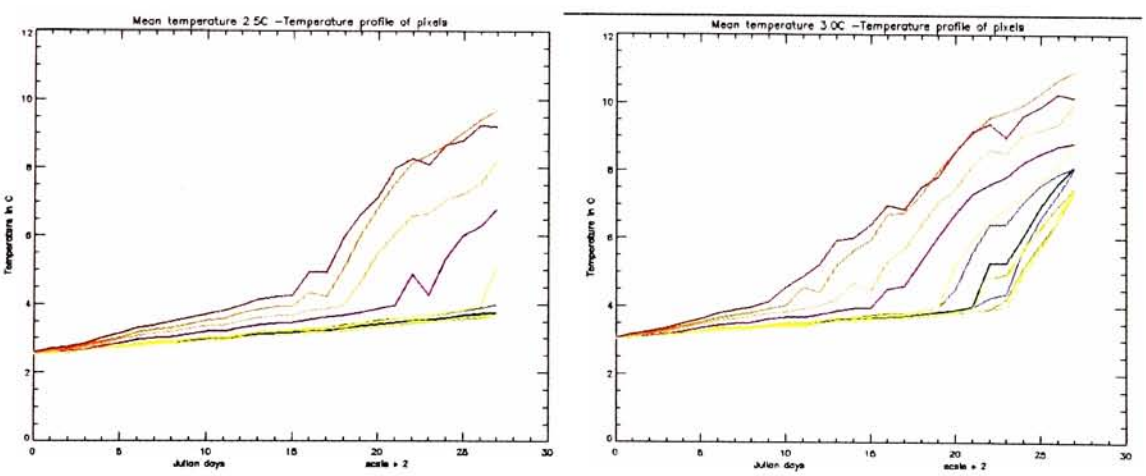


e) f)

Figure 3.5: Mean temperature of the lake during winter stratification image e)= $2.5^oC$; image f)= $3^oC$

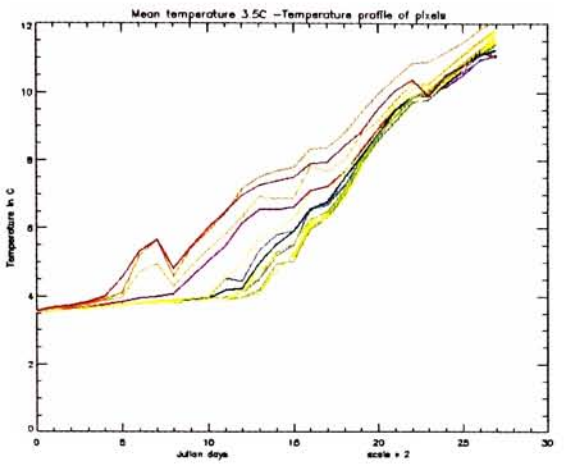


Figure 3.6: Mean temperature of the lake during winter stratification image g)= $3.5^oC$

**Observations**

- The pixels B to G behave similarly when the mean temperature of the Lake during winter stratification is less than or equal to $2.5^oC$.
- The temperature of pixels B to G have a very similar heating rate and the temperature rises by 1 degree during the 60 Julian days when the mean temperature is less than or equal to $2.5^oC$.
- When the mean temperature of the lake during the winter stratification is greater than $2.5^oC$ there is rather a higher heating rate shown in all the pixels
- It could be clearly seen that the Northern shore heats up much faster than the Southern shore (Rodgers, 1971)
- It could be observed that there is a large temperature increase in the entire lake when the mean temperature of the lake is increased. The above was observed in the laboratory experiments mentioned in the previous chapters.

### 3.1.5 Case Study 2 : Changing the Cloud Cover

Several case studies were conducted by changing the cloud percentage over the lake. The cloud insulation would directly affect the amount of Long Wave (LW) and Short Wave (SW) energy onto the lake affecting the amount of heat onto the surface of the lake. The case following studies were conducted:

1. By having a 0% cloud cover over the lake during the entire time of simulation.
2. By having a 50% cloud cover over the lake during the entire time of simulation.
3. By having a 100% cloud cover over the lake during the entire time of simulation.
4. By reducing the observed cloud cover by 50% for the entire time of simulation.

The temperature during the winter stratification was assumed to be $2^oC$ for all the above case studies.

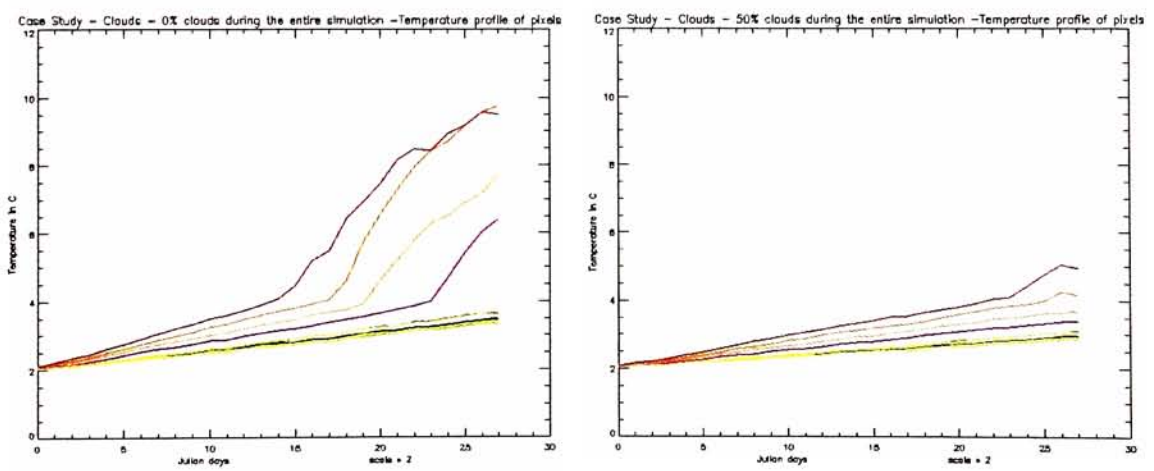


a) b)

Figure 3.7: Case study 2 -Cloud cover over the lake during the entire time of simulation image h)= 0%;image i)50%

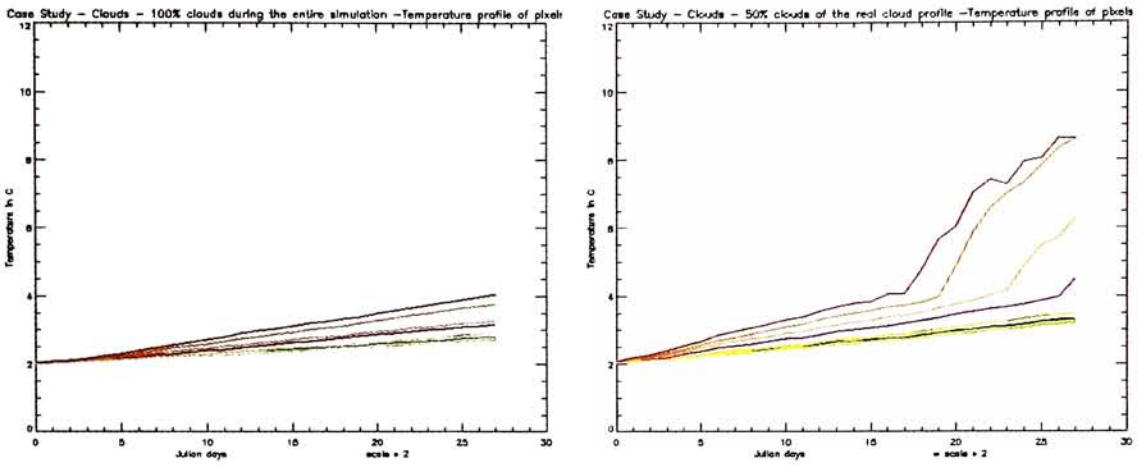


a) b)

Figure 3.8: Case study 2 -Cloud cover over the lake during the entire time of simulation image h)= 100%;image i)50% of the real cover

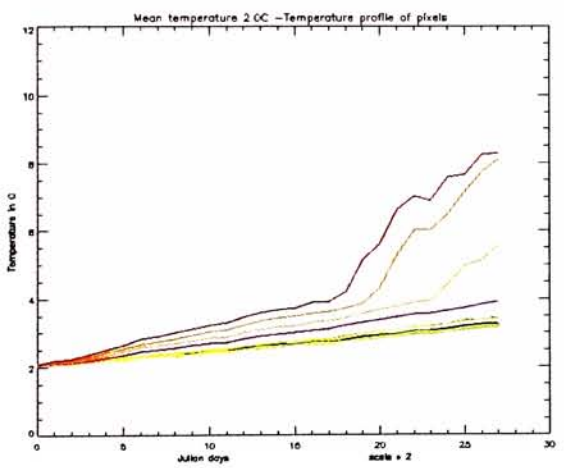


Figure 3.9: Temperature profile of the pixels with real data - for comparison

**Observations**

- The variation of the cloud cover doesn't cause a significant change during the initial stages of the simulation
- When a 100% cloud cover was imposed during the entire simulation there was a steady linear increase in the surface temperature of the entire lake. The pixels in the shallow region namely A and I to K gets heated faster than the other pixels. Because The reflected light is said to have more long-wave radiation which heats the shallow region of the lake.
- When a 50% cloud cover was imposed a steady linear increase in the surface temperature of the lake was observed except during the latter stages of the simulation. The gradients of the curves were larger than when a 100%cloud cover was imposed. There was a rather higher increase in the gradient in the pixels close to he shore.
- The absence of the could cover ( 0% during the entire simulation)causes the temperature to rise to large values especially for pixels A and I to K during the latter stage of the simulation.
- Therefore it could be concluded that the temperature of the shallower regions are very sensitive to the variation of the could cover.
- When the cloud cover was reduced by 50% of it's original amount a clear increase in temperature during the latter stages of the simulation was visible.
- It is also evident that the cloud cover is a very important factor during the latter stages of the thermal bar formation.

### 3.1.6 Case Study 3 : Changing the wind speed during the entire simulation

The wind speed of the hourly weather data was reduced by 50% during the entire simulation.

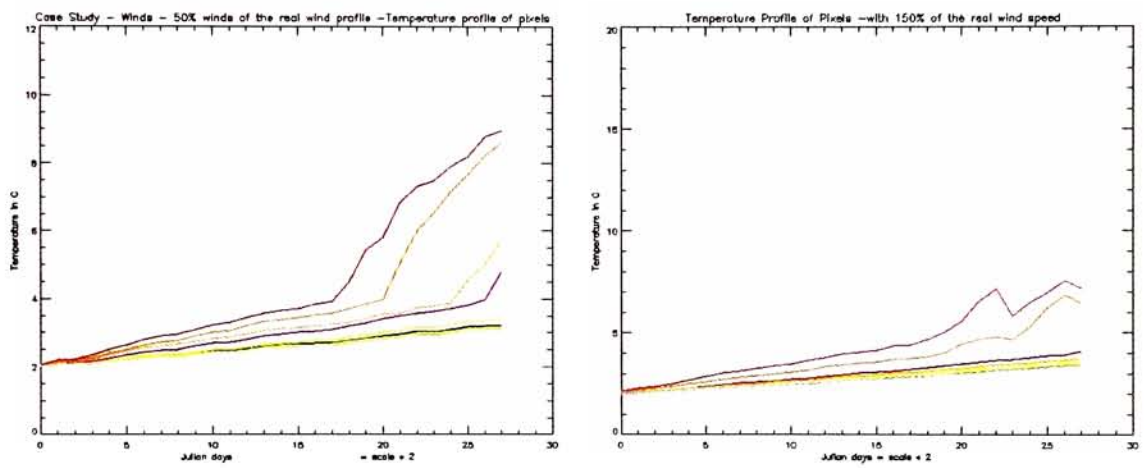


l) )

Figure 3.10: Case study 3 -Changing the wind speed during the entire simulation l)reduced by 50% m) increased by 50%

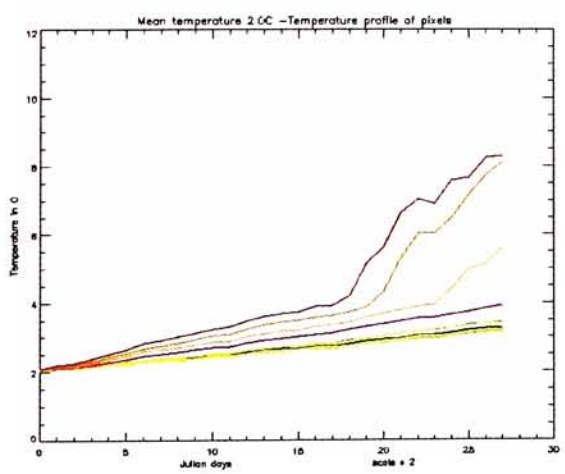


Figure 3.11: Temperature profile of the pixels with real data - for comparison

### Observations

When the wind was decreased by 50% the temperature increases were rather smother with less wiggles in the temperature profiles. No significant increase or decrease in the final temperatures were observed. When the wind was increased by 50% the evaporation increased which cooled the surface of the lake. Hence the temperature has decreased.

### 3.1.7 Case Studies With Real Bathymetric Data of Lake Ontario

The following variations were included in the case studies

1. Varying of horizontal and vertical resolution of the Bathymetric data.
2. Varying the temperature at which the lake gets stratified during winter.
3. The wind speed for a certain period.
4. The weather station at which the hourly surface meteorological data is obtained.

#### Integration of inflow and out flow

Several case studies were conducted around the integration of the inflow and outflow and varying the temperature hourly of the inflow and outflow

#### Methods of Analysis

Two methods were used to compare the above case studies:

1. Plot the variation of the area less than or equal to $4^oC$ of layers of water with depth. The blue colour represents the surface layers while the red represents the layers towards the bottom of the lake.The area within the thermal bar (less than or equal to $4^oC$) is a good gauge of the thermal bar propagational speed. The two phases of the propagational speeds could be observed in the graphs. It was decided to observe the area less than or equal $4^oC$ as the temperature ranges less than the above were very noisy.

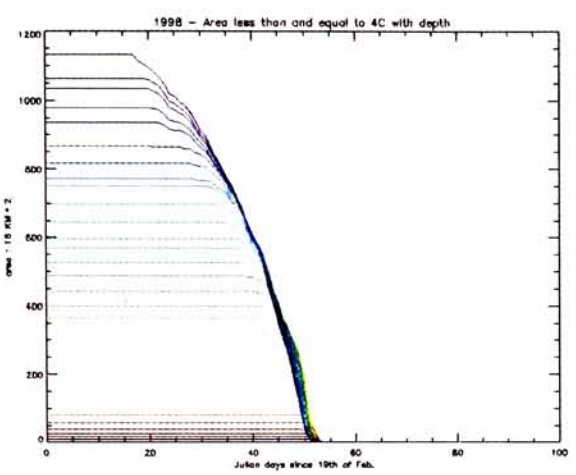


Figure 3.12: *a*)Example of a graph with area less than or equal $4^oC$ with depth

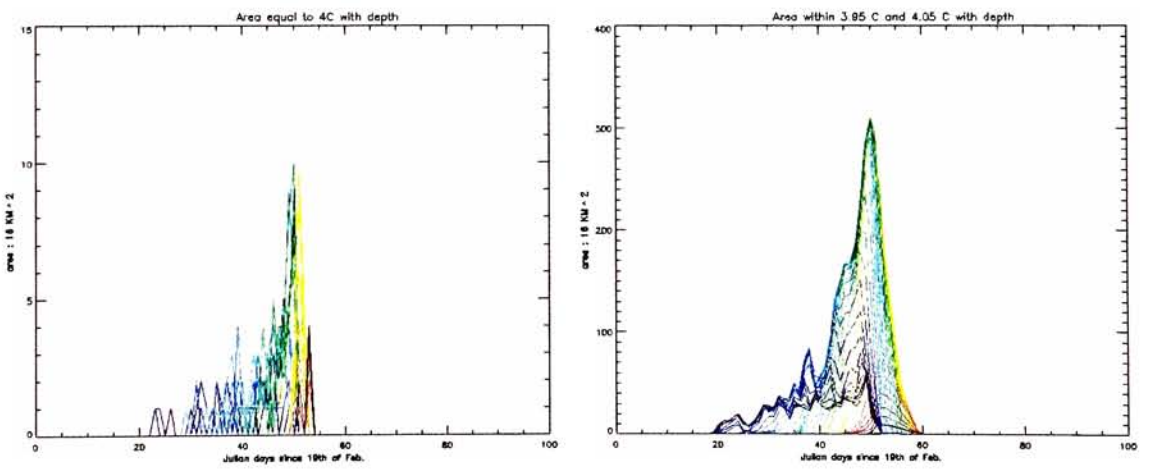


b) c)

Figure 3.13: b)Variation area of the layers where the temperature is equal to $4^oC$; image c)Area of the layers with temperature within the values $3.95 - 4.05^oC$

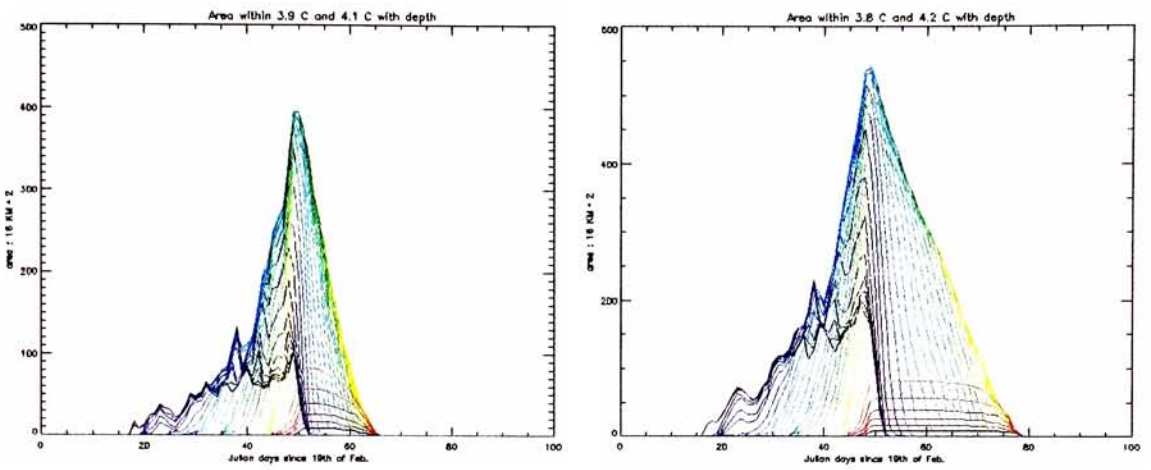


d) e)

Figure 3.14: d)Variation of area of the layers with temperature within the values $3.9-4.1^oC$ e)Variation of area of the layers with temperature within the values $3.8-4.2^oC$

2. Variation of temperature with time of selected surface pixels over the lake. The pixel profile for each of the case studies show how each parameter would affect specific subsections of the lake.

### 3.1.8 Case Studies for 1997 - March 15th to 31st August 1997 : without inflow and outflow.

The starting date for the simulation was selected by going through an archive of low resolution NOAA images. Using the above, the date on which the lake surface was approximately at an iso-thermal temperature of $2^oC$ was selected.

Hourly surface meteorological data and radiosonde data were downloaded and formatted to the required format.The following graphs show how the surface area within the thermal bar varies with time and the temperature profile of selected pixels.

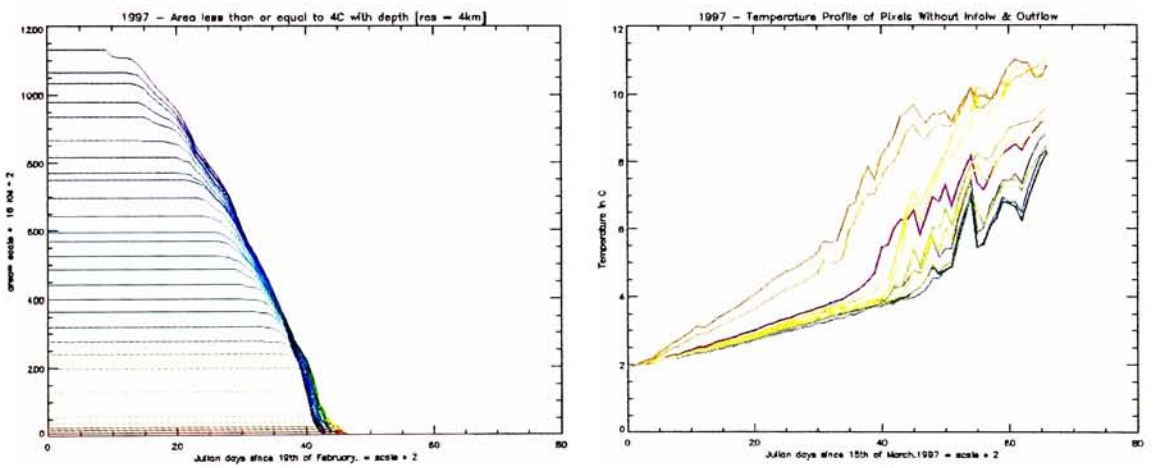


a) b)

Figure 3.15: Case Studies for 1997 - March $15^{th}$ to July $31^{st}$ August 1997 : without inflow and outflow. a)Area within the thermal bar; image b)pixel profiles

#### Observations

It could be clearly seen that the surface pixels of shallow water tends to be heated up faster than the central pixels. It was also clear that the North-Eastern surface pixels are always warmer than the South-western Surface pixels (Rodgers, 1971)

### 3.1.9 Case Studies for 1997 - March $15^{th}$ to July $31^{st}$ 1997 : varying the initial conditions

**Varying the temperature at which the lake gets stratified during the winter**

Varying the mean temperature of the lake during the winter stratification(with no inflow and outflow). The literature by (Rodgers, 1971), (Farrow, 1994) (Farrow, 1995) states that the mean temperature of the lake during the winter stratification is $2^oC$. Also the literature states that the propagational speed of the thermal bar is inversely proportional to the mean iso-thermal temperature of the lake during the winter stratification. The above study was conducted to verify the temporal propagation.

1. Assuming the whole lake is at an iso-thermal temperature of $1^oC$ during the winter stratification

2. Assuming the whole lake is at an iso-thermal temperature of $3^oC$ during the winter stratification

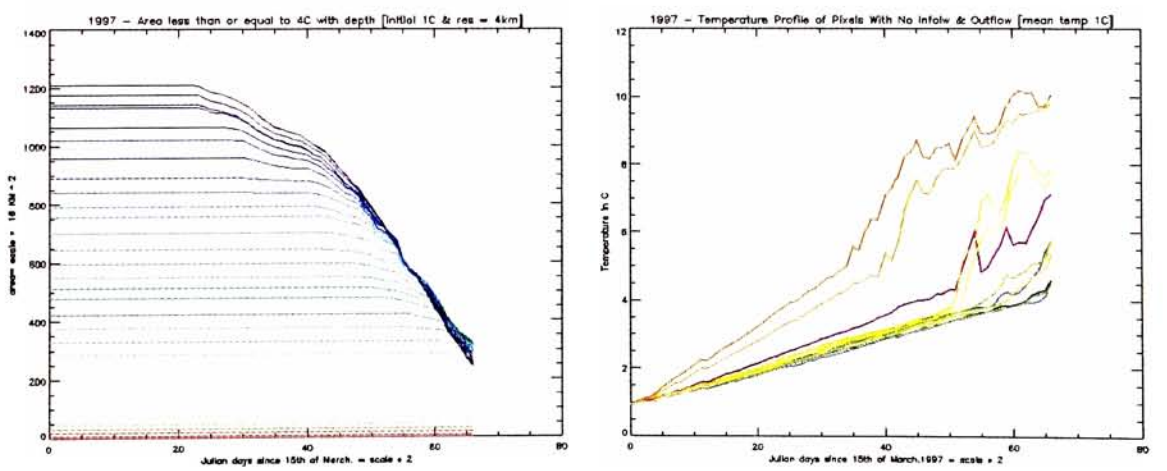


a) b)

Figure 3.16: Assuming the whole lake is at an iso-thermal temperature of $1^oC$ during the winter stratification a)Area within the thermal bar; image b)pixel profiles

### Observations

When it was assumed that the mean temperature of the lake is $1^oC$ during the winter stratification, the entire lake is much colder. Implying the rate of increase of the temperature of the pixels in the surface is much smaller.

The above condition affected the surface pixels of the shallower water the least. As the difference in temperature is less than $1^oC$. The temperature profiles of the pixels when the mean temperature is $1^oC$. The temperature profiles of the above case study tends to be less noisy and more linear.

### Varying the the wind speed for one month

The wind was increased to a constant value of $12ms^{-1}$ through out the month of June with as the wind being South-West.

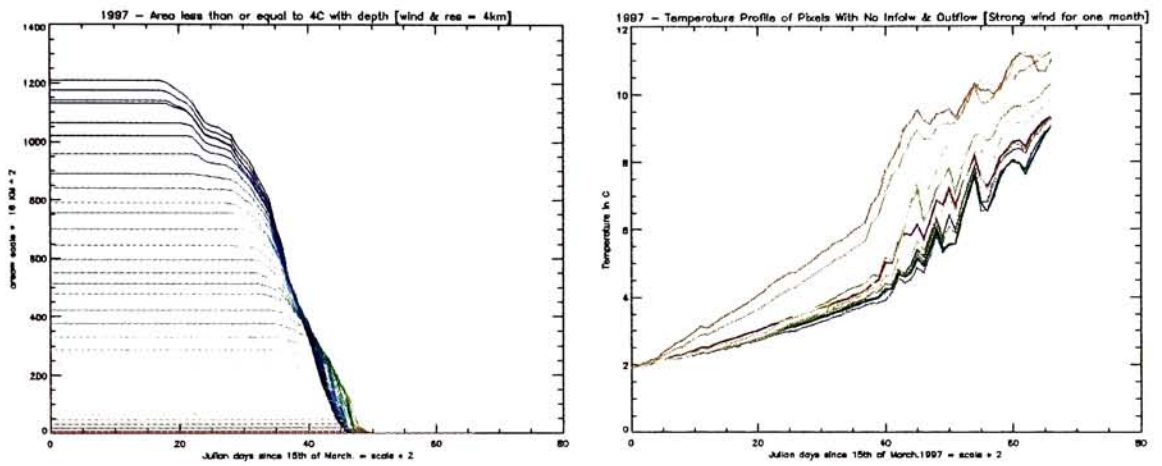


e) f)

Figure 3.17: Varying the the wind speed for one month e)Area within the thermal bar; image f)pixel profiles

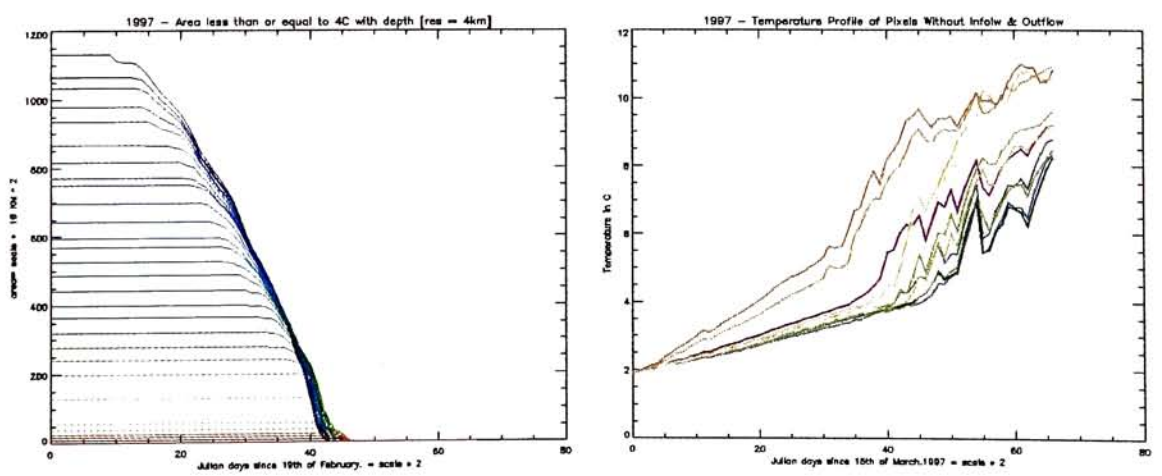


a) b)

Figure 3.18: Case Studies for 1997 - March $15^{th}$ to July $31^{st}$ August 1997 : without inflow and outflow. For comparison a)Area within the thermal bar; image b)pixel profiles

### Observations

As the winds were assumed to blow from the South-West the pixels along the South-Western shore tends to be effected the most. It is also clear that a strong gust of wind has increased the overall surfce area within the thermal bar. The surface temperature at the North-Western shore was not effected as much as the Southern.

### 3.1.10 $15^{th}$ March to $31^{st}$ July 1997- With inflow and outflow at Niagara and St. Lawerence.

An inflow and outflow of $7000m^3s^{-1}$ was integrated at specific inflow and outflow locations of the lake. The variations of the surface temperature with time is represented in the following graphs.

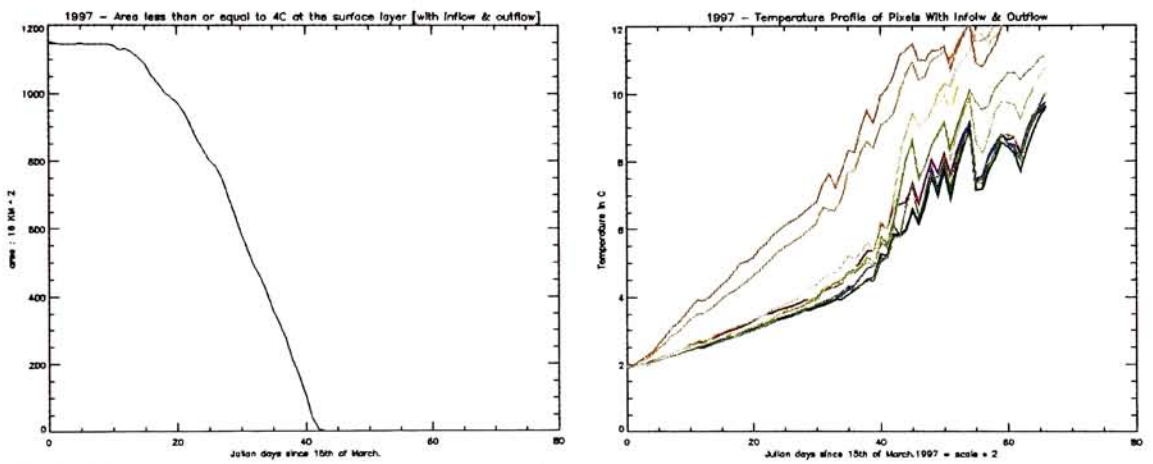


a) b)

Figure 3.19: March $15^{th}$ to $31^{st}$ July 1997- With inflow and outflow at Niagara and St. Lawerence.a)Area within the thermal bar- of the surface layer; image b)pixel profiles

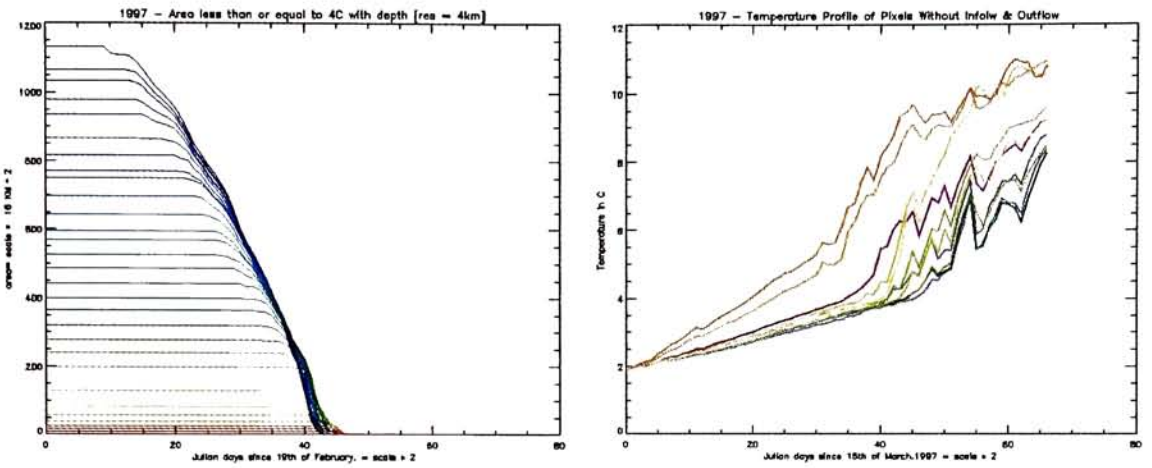


a) b)

Figure 3.20: Case Studies for 1997 - March $15^{th}$ to July $31^{st}$ August 1997 : without inflow and outflow. - For comparison a)Area within the thermal bar; image b)pixel profiles

### Observations

The inflow and outflow increased the overall temperature of the surface pixels. The integration of inflow and outflow only effected when the temperature that was greater than $4^oC$ as the are within the thermal bar did not differ much in the surface layer other than close to the the Niagara river.

### Comparison of the Case Studies With and Without Inflow

There is a clear difference within the thermal bar. The pixel profiles show a dramatic increase in the temperature. Relative temperature turbulances are seen in the South-Western part of the lake due to the inflow. It seems that the North-Eastern pixels of the lake gets effected the least by the integration of the inflow and the outflow. The temperature profiles of the North-Eastern pixels retain the same shape, while the South-Western pixel temperature profiles tend to be noisy. The relative increase in temperature of the North-Eastern pixels are much higher than the South-western pixels.

### 3.1.11 March $15^{th}$ to July $31^{st}$ 1997- With bathymetry data of $2km$ resolution – resampled from $3km$ resolution bathymetry data.

The sensitivity of the model to the horizontal resolution of the bathymetric data were studied by increasing the resolution to $2km$ while keeping the vertical resolution the same. The $2km$ bathymetric were obtained by resampling the original bathymetric data obtained from NOAA of $3km$ horizontal resolution.

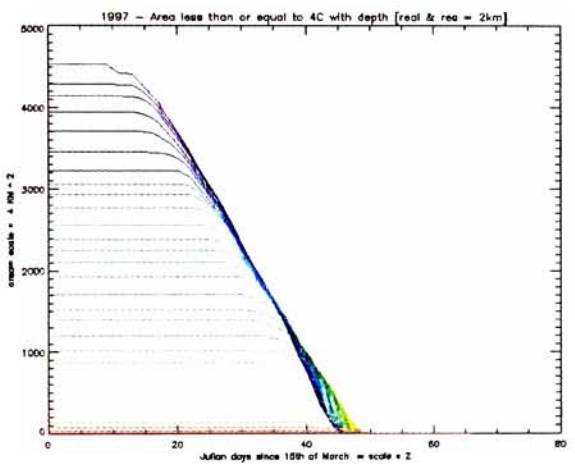


Figure 3.21: March $15^{th}$ to July $31^{st}$ 1997- With bathymetry data of $2km$ resolution – resampled from $3km$ resolution bathymetry data.a)Area within the thermal bar

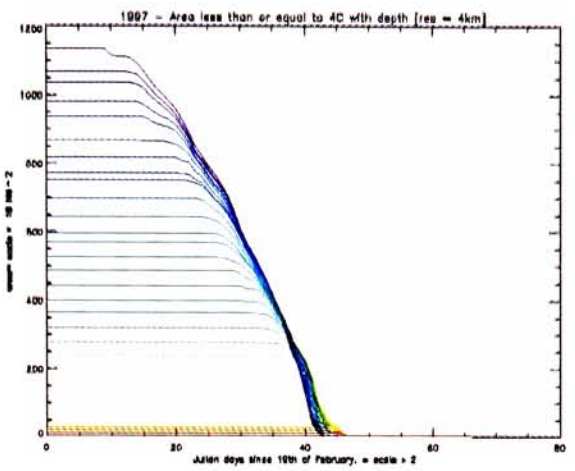


Figure 3.22: March $15^{th}$ to July $31^{st}$ 1997- With bathymetry data of $4km$ resolution – resampled from $3km$ resolution bathymetry data. For comparison a)Area within the thermal bar

### Observation

There is a variation between the $4km$ resolution and the $2km$ resolution bathymetric case studies. It seems that the $2km$ resolution bathymetric data increased the propagational speed of the thermal bar. Which made the thermal bar disappear sooner by about 5 days. It had to be examined whether the above was due to the bathymetry or due to the fact that the model itself was sensitive to the grid size. Hence the next case study was designed such that the bathymetry data of $2km$ resolution were obtained by resampling the $4km$ bathymetric grid instead of the $3km$ bathymetric grid.

### 3.1.12 March $15^{th}$ to July $31^{st}$ 1997- With bathymetric data of 2km resolution resampled from 4km resolution bathymetric data.

The $4km$ resolution bathymetry data were resampled in ARC/INFO( GRID) to obtain the 2km bathymetric gridded data.

**Observation**

According to the above it seems that the propagational speed is lower than the previous case study but it is faster than the 4km bathymetric data. Hence it could be concluded that the increase in the propagational speed of the thermal bar is partially due to the bathymetric variation of the sampling data and also due to the grid size that's been used in the mathematical calculations.

### 3.1.13 Case Studies for 1998 - $19^{th}$ of February to $19^{th}$ of August 1998 : without inflow and outflow - Surface Meteorological data from Buffalo Weather Station

The starting date was selected by going through an archive of low resolution NOAA images. Using the above the date on which the lake surface showed a constant iso-thermal temperature of $2^oC$ (throughout a period of time) was chosen to be the date at which the lake was stratified. Hourly surface meteorological data from the Meteorological station in Buffalo and radiosonde data from Buffalo were downloaded and formatted to the required format.The following graphs show how the surface area within the thermal bar varies with time and the temperature profile of selected pixels.

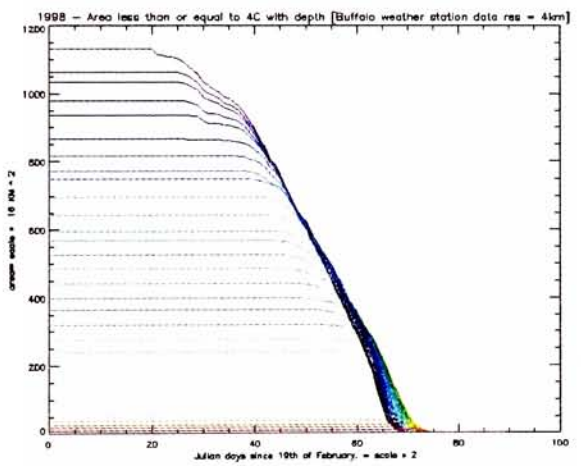


a) b)

Figure 3.23: Case Studies for 1998 - 19th of February to 19th of August 1998 : without inflow and outflow - Surface Meteorological data from Buffalo Weather Station a)Area within the thermal bar; image

### 3.1.14 Case Studies for 1998 - $19^{th}$ of February to $19^{th}$ of August 1998 : without inflow and outflow - Surface Meteorological data from Fulton Weather Station

The purpose of the above case study was to see how sensitive the hydrodynamic model (ALGE) is to the spatial location of the weather station from which the surface meteorological data is obtained. Hourly surface meteorological data was obtained from the Fulton meteorological station for the above period of study and integrated to ALGE.

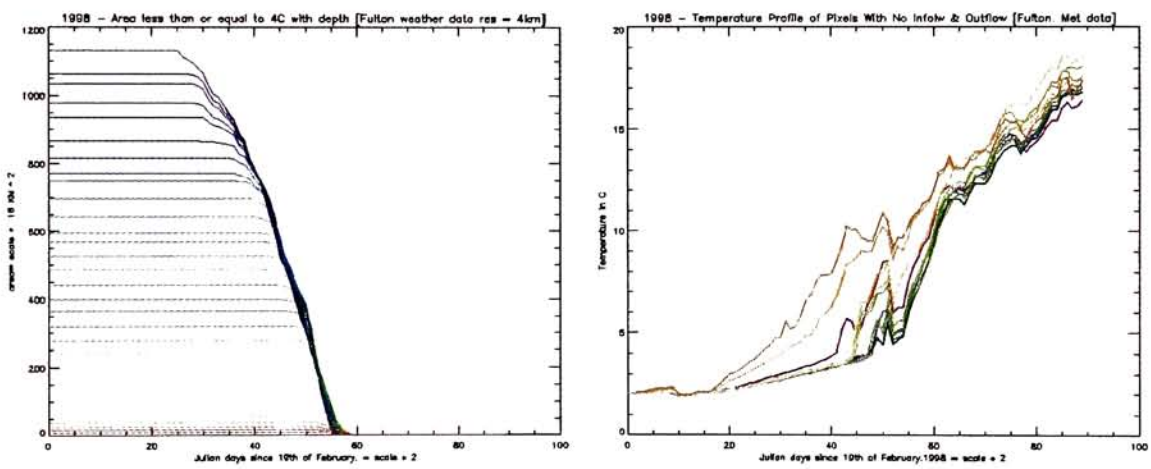


c) d)

Figure 3.24: Case Studies for 1998 - $19^{th}$ of February to $19^{th}$ of August 1998 : without inflow and outflow - Surface Meteorological data from Fulton Weather Station c)Area within the thermal bar; image d)pixel profiles

#### Observations

The formation and the propagation of the thermal bar with the weather data from Fulton increased the propagational speed of the bar. Which made the thermal bar to form and disappear much slower than with Buffalo weather data.

It was clearly seen that the spatial location had a clear impact on the formation and

the propagation of the thermal bar. It was concluded that the hydrodynamic model ALGE was sensitive to the spatial location of the weather station, hence weather data from seven weather stations located around Lake Ontario were chosen so that the data could be spatially interpolated and integrated to the model.

### 3.1.15 Case Studies for 1998 - $19^{th}$ of February to $19^{th}$ of August 1999 : without inflow and outflow - With Spatially interpolated data from 7 meteorological stations around Lake Ontario

Figure 3.25: Spatial Locations of the seven Weather stations

Weather data from seven station were formatted and spatially interpolated using the Delaunay triangulation methodology. The wind direction and speed were interpolated by resolving it to horizontal and vertical components. The mean value of the spatially interpolated data were used as input to the Hydrodynamic model ALGE.

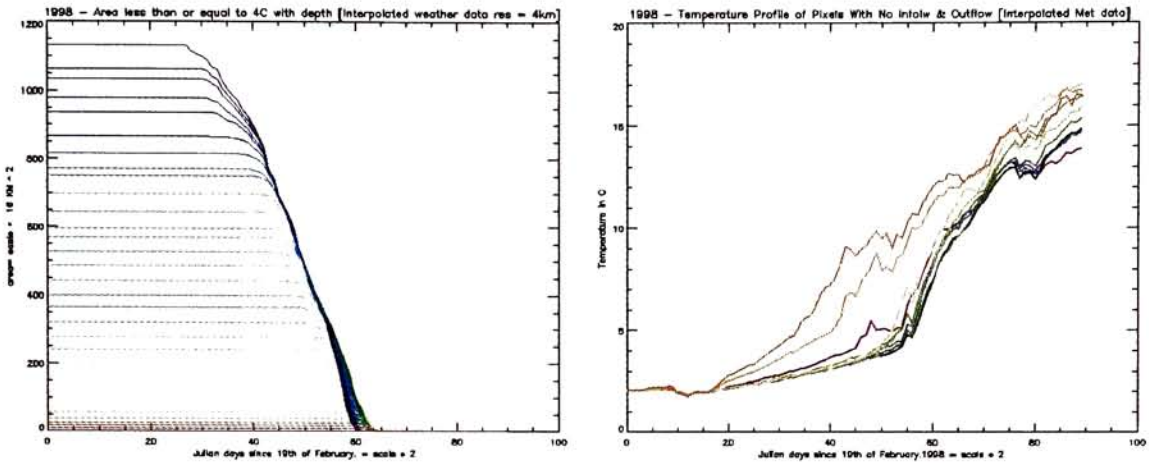


e) f)

Figure 3.26: Case Studies for 1998 - $19^{th}$ of February to $19^{th}$ of August 1998 : without inflow and outflow - Using Spatially interpolated Surface Meteorological data from Seven Weather Station e)Area within the thermal bar; image f)pixel profiles

## Comparison

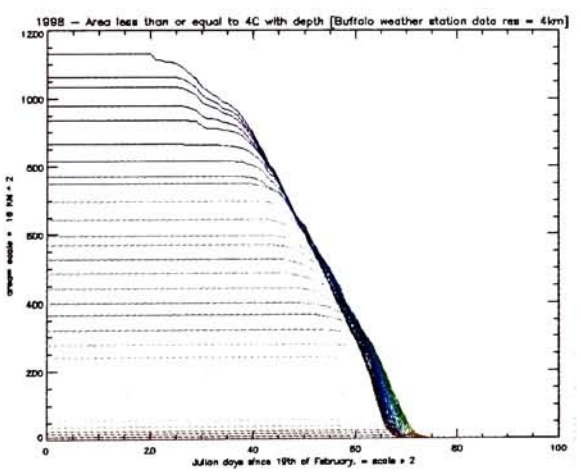


Figure 3.27: Case Studies for 1998 - $19^{th}$ of February to $19^{th}$ of August 1998 : without inflow and outflow - Surface Meteorological data from Buffalo Weather Station image)Area within the thermal bar;

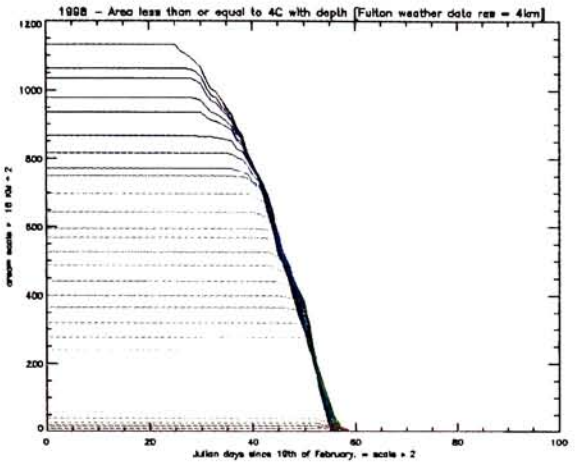


Figure 3.28: Case Studies for 1998 - $19^{th}$ of February to $19^{th}$ of August 1998 : without inflow and outflow - Surface Meteorological data from Fulton Weather Station image)Area within the thermal bar;

### Observations

The spatially interpolated weather data from seven meteorological stations produced a propagational speed that was less than that of Fulton weather data and much greater than the speed induced by the Buffalo weather data.

### 3.1.16 Case Studies for 1998 - $19^{th}$ of February to $19^{th}$ of August 1989 : without inflow and outflow - Increased vertical resolution of $3.6m$

The baseline ALGE code was capable of simulating 36 vertical layers. The number of vertical layers were increased to 74 layers which increased the vertical resolution to $3.6m$. The above case study was conducted to observe the detailed temperature changes at the Niagara Plume and to see how important it is to increase the vertical resolution of the lake.

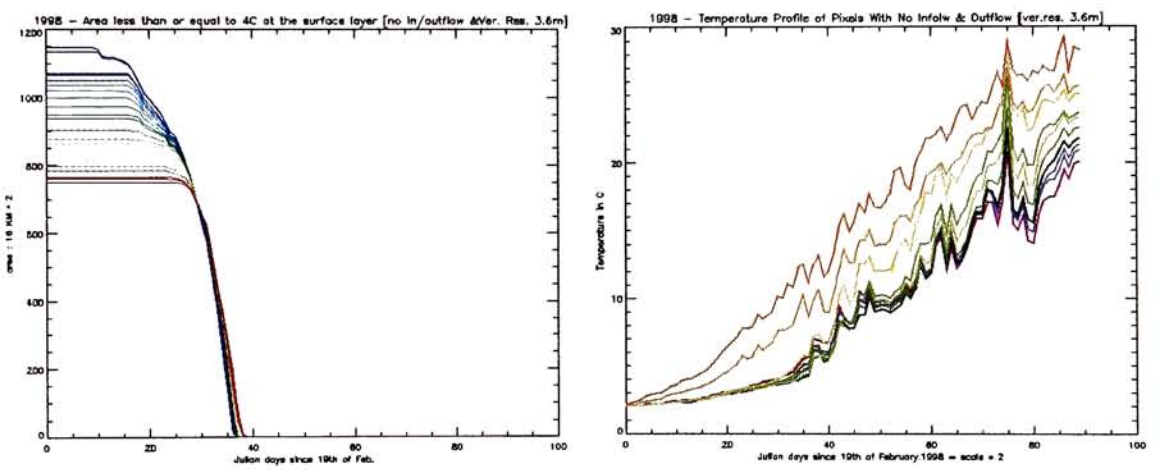


a) b)

Figure 3.29: Case Studies for 1998 - $19^{th}$ of February to $19^{th}$ of August 1998 : without inflow and outflow - Increased vertical resolution of $3.6m$: a)Area within the thermal bar of the first 25 layers; image b)pixel profiles

#### Observation

The increase of the vertical resolution introduced some variation and also increased the propagational speed of the thermal bar. Some eddies close to the Niagara plume were seen very clearly. These eddies were not visible in the lower vertical resolution runs. The overall speed of the thermal bar increased which made the thermal bar to form and disappear faster. It is also clear that the surface pixels gets heated up much faster when the vertical

resolution is increased. Therefore it could be concluded that ALGE is more sensitive to the vertical resolution than the horizontal resolution.

### 3.1.17 Study of the Niagara plume

It was decided to study a part of the lake at a higher resolution of $100m$. For the above a part of the bathymetric data was clipped and converted to a TIN (Triangular Irregular Network) for resampling at a finer resolution. Once the above was done the bathymetry was integrated to the model and simulated with appropriate boundary conditions for a few hours.

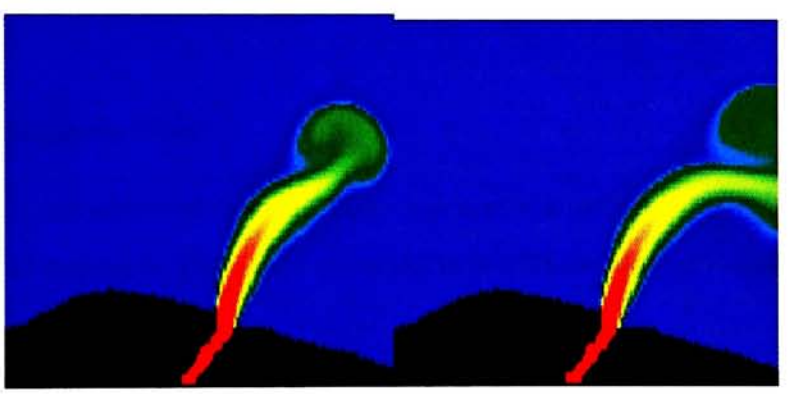

a) b)

Figure 3.30: The Niagara Plume after image n1) 12 hours of simulation n2)18 hours of simulation

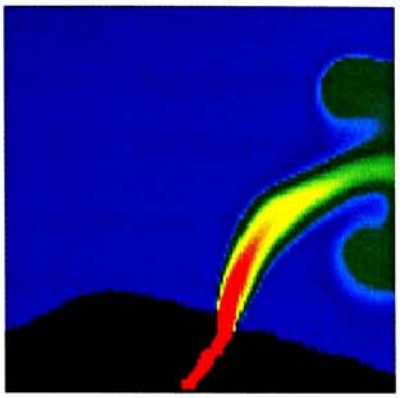

Figure 3.31: The Niagara Plume after 24 hours of simulation

### Observations

It was observed that the Niagara plume is sensitive to the South-Western winds and behaves according to the plume observed in the Thermal High resolution images.

### 3.1.18 Case Studies for 1998 - $19^{th}$ of February to $19^{th}$ of August 1989 : Interpolated weather data - with the integration of hourly temperature profile of the inflow at Niagara

In all the previous case-studies the inflow and outflow had a constant temperature of $5^oC$ throughout the entire year. Which was incorrect as the low temperature at the Niagara towards the late summer was clearly seen in the outputs. Therefore an hourly Temperature profile of a river in New York East river was integrated to ALGE.

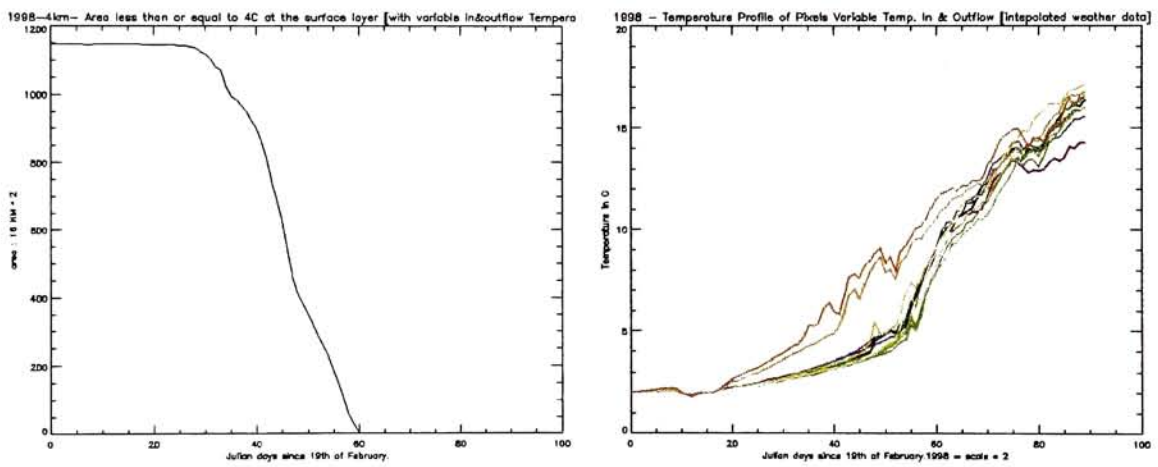


a) b)

Figure 3.32: Case Studies for 1998 - $19^{th}$ of February to $19^{th}$ of August 1989 : Interpolated weather data - with the integration of an hourly temperature profile of the inflow at Niagara a)Area within the thermal bar; image b)pixel profiles

#### Observations

There was a clear difference at the Niagara plume in the outputs as the temperature of the inflow increased as the temperature of the lake increased. A clear impact on the thermal bar was seen from the very beginning of the formation stages of the thermal bar.

### 3.1.19 Case Study for 1997 through 1998 - $15^{th}$ of March 1997 to the $19^{th}$ of August 1989 - Buffalo weather data - with the integration of hourly temperature profile of the inflow at Niagara

The 1997 data files, the 1998 data files and the weather data for the months inbetween were combined for the above case study. The main intention of the above case-study was to observe how well ALGE was able to predict the lake temperature during the Fall and Winter months. The above was feasible due to the fact that the Lake didn't freeze during the above period.

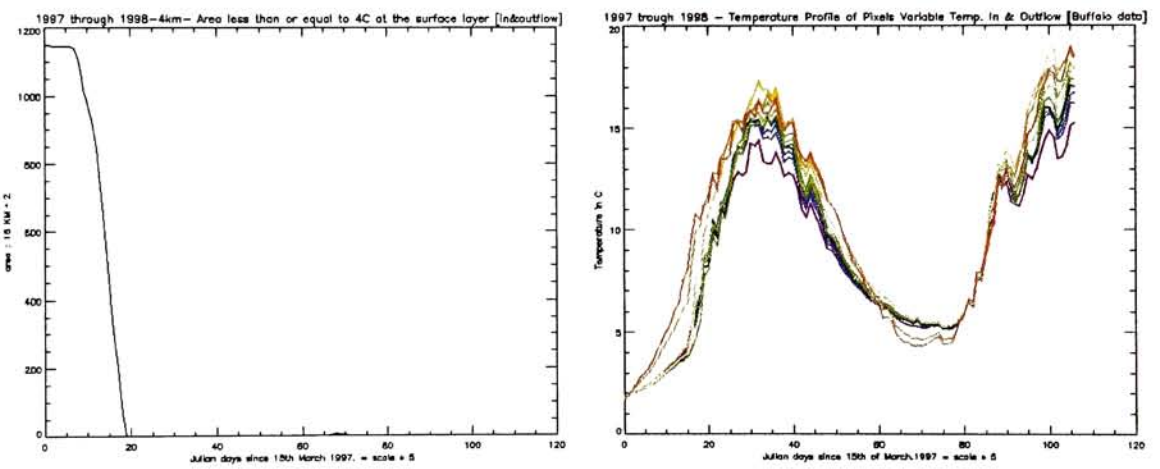


a) b)

Figure 3.33: Case Study for 1997 through 1998 - $15^{th}$ of March 1997 to the $19^{th}$ of August 1989 - Buffalo weather data - with the integration of an hourly temperature profile of the inflow at Niagara a)Area within the thermal bar; image b)pixel profiles

#### Observations

It was evident that ALGE was simulating the hydrodynamics of the lake correctly. Since the temperature of the lake during the winter and summer stratifications (turnover) of the lake remained at a constant temperature for a couple of days.

It was also observed that the entire lake is at a bout $5^oC$ during the 1998 winter stratification. Which is rather high as a temperature of the lake during the winter turn over.

Due to the above observation it was decided to integrate weather data from a station situated at a higher latitude. The intention was to observe whether the colder weather data would decrease the turnover temperature of the lake.

### 3.1.20 Case Study for 1997 through 1998 - $15^{th}$ of March 1997 to the $19^{th}$ of August 1989 - Fulton weather data - with the integration of hourly temperature profile of the inflow at Niagara

Weather data from the Fulton weather weather station was integrated to the model during the above period.

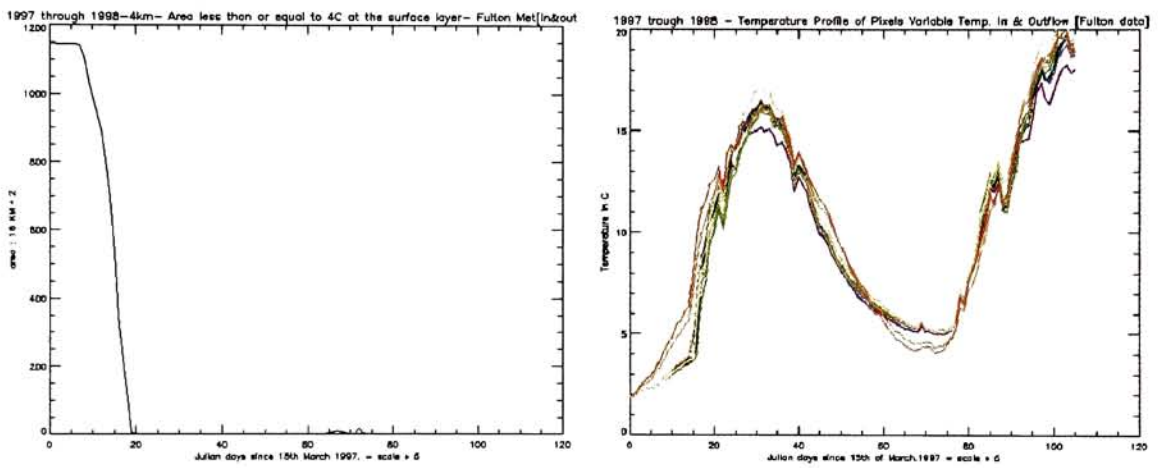


a) b)

Figure 3.34: Case Study for 1997 through 1998 - $15^{th}$ of March 1997 to the $19^{th}$ of August 1989 - Fulton weather data - with the integration of hourly temperature profile of the inflow at Niagara - with the integration of an hourly temperature profile of the inflow at Niagara a)Area within the thermal bar; image b)pixel profiles

#### Observations

It was clear that the temperature during the winter stratification remained at the same temperature as observed with Buffalo weather data. Hence it could be concluded that the lake tends to contain more energy that it should during the winter. The above could be due to either the lake gets heated up more than it shouldn't be (hence the insulation factor should be dealt with) or it does not account for all the energy losses during the winter.

It could be also observed that the model simulates the winter stratification for 1998 around the same times observed in satellite imagery. By inspecting AVHRR low resolution satellite imagery it was decided that the surface was at an isothermal temperature for 1998 around the $19^{th}$ of February. The model was given that the winter stratification time for 1997 is around the $15^{th}$ of March 1997 (after inspecting satellite images for 1997). With the above date for 1997 and the weather data it predicted the winter stratification date to be around the $25^{th}$ of February 1998. Hence it is evident that ALGE simulates the hydrodynamics accurately.

### 3.1.21 Case Studies for 1999 - $18^{th}$ of March to $1^{st}$ of August 1999 : Buffalo Weather Data - with the integration of hourly temperature profile of the inflow at Niagara

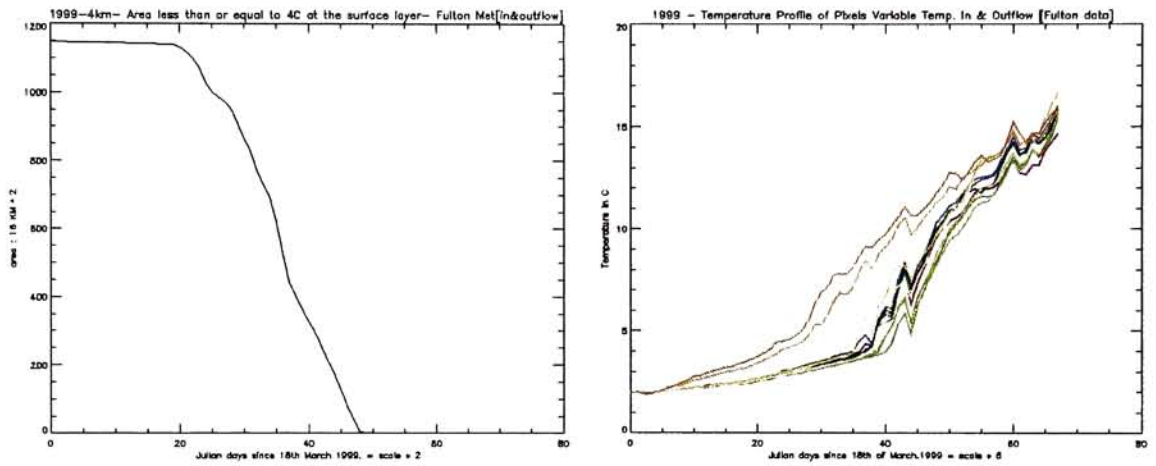


a) b)

Figure 3.35: Case Studies for 1999 - $18^{th}$ of March to $1^{st}$ of August 1999 : Buffalo Weather Data - with the integration of hourly temperature profile of the inflow at Niagara a)Area within the thermal bar; image b)pixel profiles

## 3.2 Comparison of ALGE with satellite images and other hydrodynamic models

### 3.2.1 Comparison of ALGE with satellite images

Low-resolution AVHRR images were used for the comparison. The cloud free AVHRR images were selected from a web site and purchased. The images were transferred from an 8mm tape to a CD. The Great Lakes region was selected and clipped using IDL. Then the clipped region was transferred to ARC/INFO and geo-referenced. Then the above image was further clipped to obtain the lake Ontario region. Once the above sequence was executed all the 5 bands of the AVHRR images were sent through ARC/INFO-GRID, to compute the temperature for per pixel basis. The following equations were used to compute the split and dual window technique.

**Split window**

$$T_s = A_0 T_{11} + A_1(T_{11} - T_{12}) + A_2(T_{11} - T_{12})(\sec\theta - 1) + A_3 \sec\theta + A_4 \qquad (3.1)$$

In the above $T_{11}$ and $T_{12}$ are the digital counts obtained from bands 4 and 5 respectively.

**Dual window**

$$T_s = A_0 T_{11} + A_1(T_{3.7} - T_{11}) + A_2(T_{3.7} - T_{11})(\sec\theta - 1) + A_3 \sec\theta + A_4 \qquad (3.2)$$

In the above $T_{3.7}$ and $T_{11}$ are the digital counts obtained from bands 3 and 4 respectively. Where $\theta$ is the sensor zenith angle. The $\sec\theta$ in the above equations were assigned as 1 by selecting cloud free images where the great lakes are in the center of the images.

### 3.2.2 Comparison of the split and dual window techniques

The above equations were used to derive the temperature from the AVHRR imagery for 1997 and 1998. The 1997 data were from NOAA-12 while the 1998 data were from NOAA-

14. The coefficients for the dual window technique were not available for NOAA-14. Hence the comparison of dual and split window technique was available only for 1997 images. The temperature derived from the Dual window technique was about 2 degrees colder than the temperature derived from the split window technique. The same temperature structure was observed in the temperature profiles derived from both the techniques. The similarity in the thermal structure was clearly seen in all the images. Several comparisons of split window and the dual window technique are saved in the attached CD.

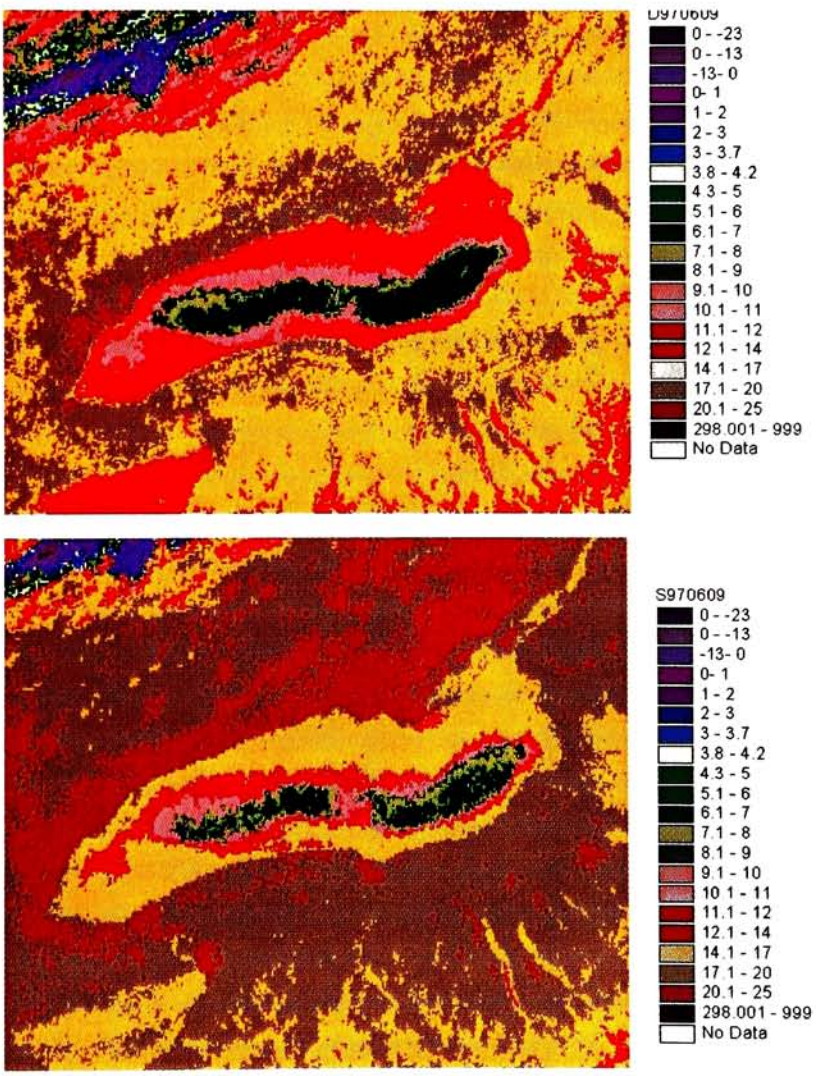


Figure 3.36: Comparison of the Split and Dual window algorithms for June 09 1997 up)Dual window bottom)split window

### 3.2.3 Comparison of Split and Dual window technique with the IMGMAP and OCNMAP algorithms

Surface temperature profiles derived from the IMGMAP and OCNMAP algorithms, were obtained from Michigan Technological University (MTU). The above temperature profiles were not available for 1997. Therefore the algorithms were compared for 1998. The MTU temperature profiles had similar surface thermal structures as the temperature profiles derived at RIT using the Dual and Split window technique. Since only the split window coefficients were available for 1998 the temperature derived from the split window technique was directly compared with the temperature profiles that were obtained from MTU. The temperature derived using the IMGMAP and OCNMAP were $1^oCto1.5^oC$ degrees colder than the temperature derived from the Split window technique. It was observed that both the above had the same temperature structure. The upwelling in the North-Western shore were seen at approximately the same times. A warm water region in the Southern shore and the impact sue to the Niagara plume is seen in both the temperature profiles.

Due to the fact that the MTUs images compared well to the Split window algorithm and had a good collection of temperature profiles over the entire year it was decided to use the temperature profiles derived by MTU to compare with the output of ALGE.

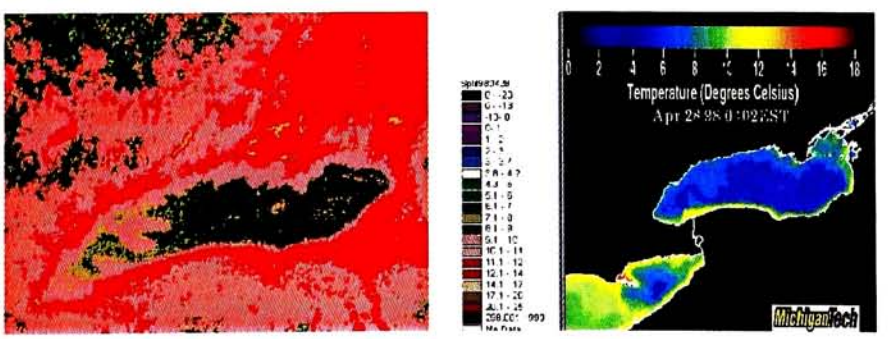


Figure 3.37: Comparison of Split window technique with the IMGMAP and OCNMAP algorithms - April 28 1998

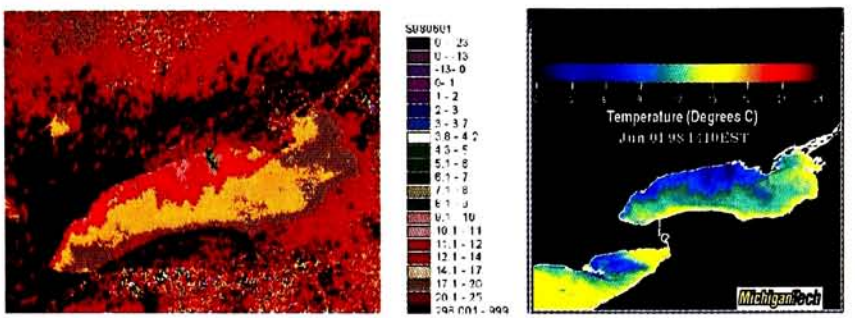


Figure 3.38: Comparison of Split window technique with the IMGMAP and OCNMAP algorithms - June 01 1998

### 3.2.4 Comparison of ALGE output with surface temperature derived from satellite imagery

ALGE output was colder than the temperature profile obtained from the satellite. Therefore it was decided to increase the temperature at which the lake gets stratified during winter to $3.25^oC$ and $3.75^oC$ from $2^oC$. It was observed that when the temperature of the entire lake during winter stratification, is $3.75^oC$, the surface temperature simulated by ALGE behave very similar to the surface temperature derived from the images. During the month of May the surface temperature derived from the imagery were very much higher than the ALGE output. But the output and images match-up again in June and July. A warm water region seen at the Southern shore starting from Niagara to the North East part of the lake is visible in the images but the above is not a prominent feature in the ALGE output. The upwelling in the North-Western part of the lake is clearly visible in both the ALGE output and the images.

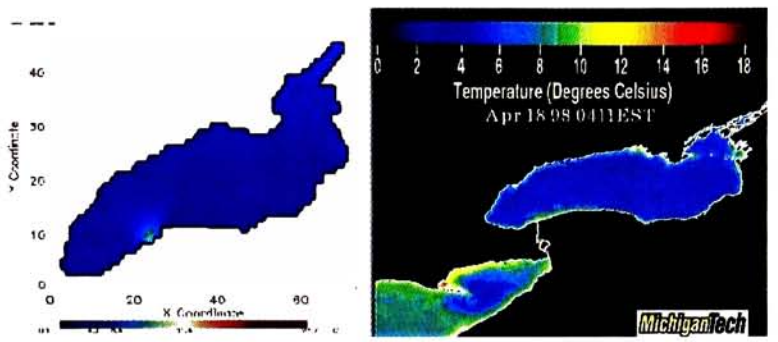


Figure 3.39: Comparison of ALGE output with surface temperature derived from satellite imagery - April 27 1998

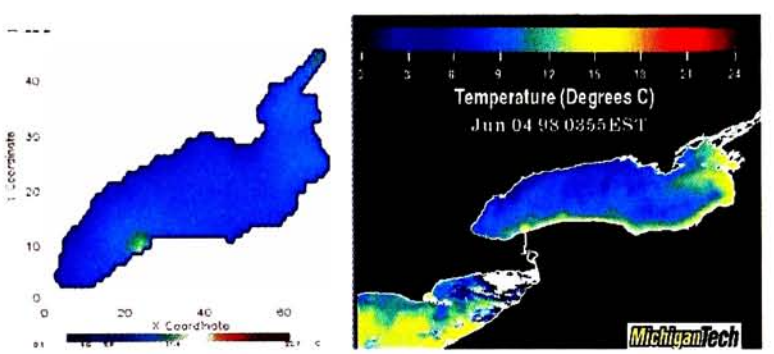


Figure 3.40: Comparison of ALGE output with surface temperature derived from satellite imagery - June 04 1998

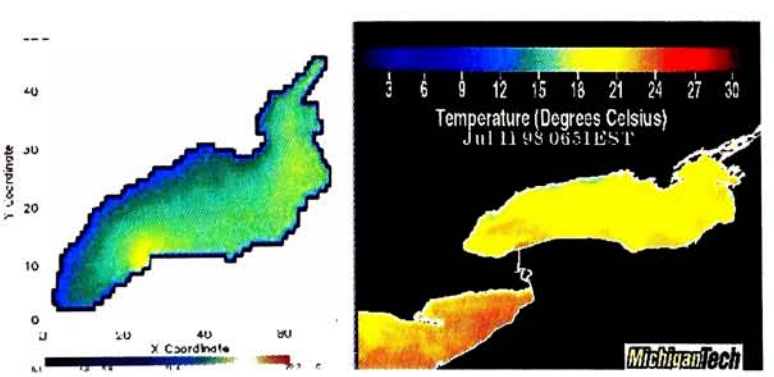


Figure 3.41: Comparison of ALGE output with surface temperature derived from satellite imagery - July 11 1998

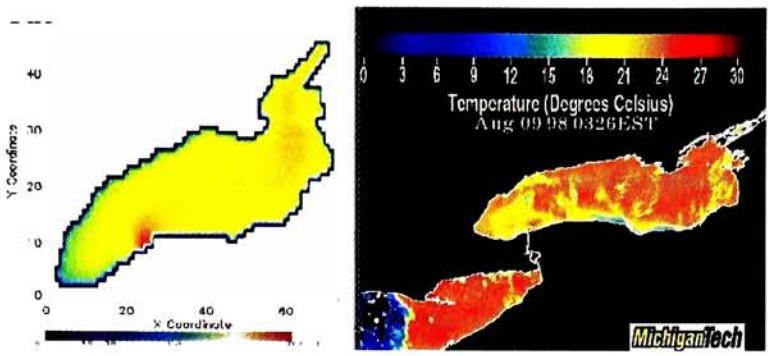


Figure 3.42: Comparison of ALGE output with surface temperature derived from satellite imagery - August 09 1998

### 3.2.5 Comparison of ALGE with the NOAA forecasting model

The forecasting model assumes that the entire lake is at a mean temperature of $3^oC$ during winter stratification on the $15^{th}$ of March for both the years 1997 and 1998. ALGE obtains the date at which the lake gets stratified from satellite images. As for ALGE it was assumed that the entire lake is at a temperature of $2^oC$ on the $15^{th}$ of March for the year 1997 and on the $19^{th}$ of February for 1998. Since ALGE assumes that the temperature during winter stratification was $2^oC$ on the $19^{th}$of February for 1998 while the forecasting model assumes it is $3^oC$ on the $15^{th}$ of March 1998, the output compares well. The position of the thermal bar and the up welling were seen at the same the same positions approximately at the same time. A stream of cold water was seen close to the Southern shore in the NOAA forecasting model. But the above was not visible in ALGE. The upwelling occurred in the North-Western shore in both the cases during the same times starting late June continuing until late July. As for 1997 ALGE and the NOAA forecasting model outputs differed considerably mainly because of the difference in the temperature of the lake during the winter stratification.

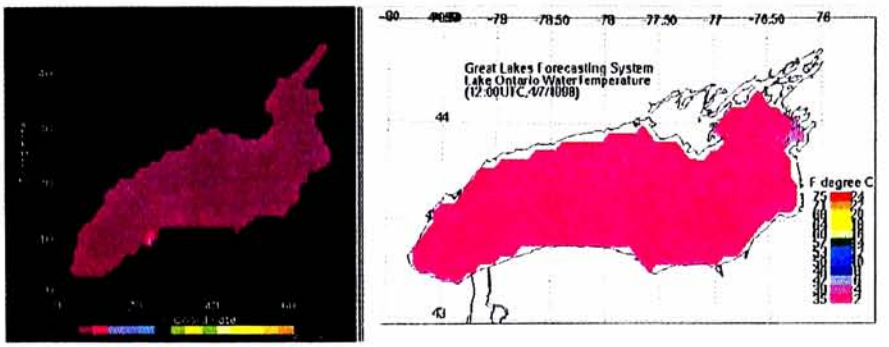


Figure 3.43: Comparison of ALGE with the NOAA forecasting model- Date $7^{th}$ April 1998

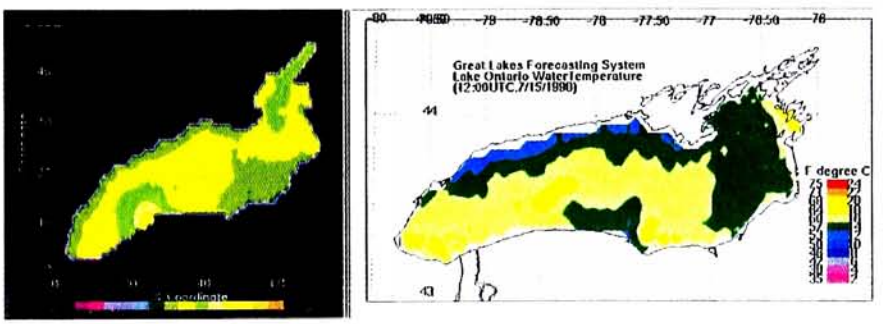


Figure 3.44: Comparison of ALGE with the NOAA forecasting model $15^{th}$ July 1998

# Chapter 4

# Conclusions and Recommendations

## 4.1 Conclusions

The following could be concluded from the case studies that were conducted in this study.

- ALGE is sensitive to the temperature during winter stratification. The bar formed earlier and disappeared faster if the temperature during the winter stratification was relatively warmer. Which confirms the statement in the literature (Elliott and Elliott, 1970) where it was observed in laboratory studies that the propagational speed was inversely proportional to the temperature difference from $4^oC$.

- ALGE simulates the cloud cover correctly under the assumption that the cloud cover is uniformly distributed. No specific spatial location is assigned to the cloud cover. It was clearly seen an increase of cloud cover made the shallower regions heat up much faster due to the increase of the reflected light. Therefore it could be concluded that the clouds seem to effect the lake spatially and temporally.

- Several case studies were conducted increasing and decreasing the wind speed during the entire simulation and by adding a very large wind for a short time period. The case studies on the wind speed clearly showed that the wind-speed has it's impact on the shallower regions and deeper regions differently. Hence we could conclude that ALGE is sensitive to the wind speed and that it is sensitive to the speed spatially and temporally.

- integration of the inflow/outflow, simulating the Niagara Plume at a higher resolution and changing the temperature at the inflow confirmed that ALGE simulates the sources and sinks correctly and that it is sensitive to the spatial locations and spatial weather conditions such as wind-speed and direction.

- ALGE was also sensitive to the spatial locations of the weather stations. Which confirms that ALGE is sensitive to the changes in the weather conditions.

- The increase in the horizontal resolution from $4km$ to $2km$ didn't effect the rate of heat transfer. The increase of the vertical resolution from $8.3m$ to $3.6m$ did cause the temperature to rise unexpectedly. The above would have to be corrected in the ALGE simulation.

- ALGE was designed to simulate from winter stratification to summer stratification. One case study was extended to go beyond the summer stratification to the next year. The above was possible because 1998 was a very warm year and it did not get cold enough during the winter for the water to freeze. The case study was initiated in 1997 during the winter stratification (the date for the above was obtained from satellite imagery) and ALGE was executed for a period of one and a half years. The interesting aspect that was observed was that the surface was at a isothermal temperature around the $25^{th}$ of February indicating a winter stratification for the following year which is 1998. The satellite images also indicated that the lake was stratified along that time. However the minimum temperature during the winter stratification is too warm for a lake such a climatic zone. Indicating that there is more energy in the lake than it should be during winter. How ever it is very important to remember that this case study was an extension of what ALGE was designed to do.

- When compared with images it was seen that ALGE output was much colder than the images. Then the temperature of it during the winter stratification was altered accordingly and was able to obtain a good comparison. Some features along the Southern shore that were visible in the satellite imagery was not visible in the ALGE output. It is evident that the output of the $3D$ hydrodynamic model (ALGE) could be directly compared with satellite imagery and always obtained a better match by changing the weather conditions or the initial conditions.

## 4.2 Recomendations

- Variable vertical resolution The above would enable one to study any part of the lake in detail instead of increasing the vertical resolution of the entire lake.

- Change the inflow rate at Niagara - At the moment the model assumes that the rate at which the water flows from Niagara is a constant value throughout the entire year. The flow rate varies from season to season hence the change in the flow rate should be taken into account.

- Comparison with images It was evident that the night time images compared well with the ALGE output because the ALGE output was generated at 1am Eastern time. The images were compared visually but it could be improved so that the ALGE output could be superimposed over the images and compared pixels vise. An error metric could be calculated for each output the following way. Let the temperature derived from the satellite images for pixel $(i, j)$ be $T_{I_{(i,j)}}$ Let the temperature derived from ALGE for pixel $(i, j)$ be $T_{A_{(i,j)}}$ The difference in the temperature per pixel $\Delta T_{(i,j)} = T_{I_{(i,j)}} - T_{A_{(i,j)}}$ The error for the entire lake $= \sum_i \sum_j \Delta T_{(i,j)}$ The above could be calculated for regions of the lake by dividing the lake into eight regions. And calculating the error for each region, then it could be determined which regions compare the best with the images, temporally. Therefore by using the above it could be noted which of the regions causes the most of the errors during the two phases of the thermal bar. Therefore accordingly different parameters could be used for the different regions and also the weather data could be altered accordingly for each of the regions to match the imagery.

- Studying the Genersey plume or any part of the lake in detail The Niagara plume was studied in detail the same could be done at any part of the lake at a higher resolution since higher resolution bathymetric data is available.

- Using more accurate bathymetric data - High resolution bathymetric data could be re-sampled to lower resolution and used it as an input to ALGE.

- Having different horizontal resolutions for different regions - A cold water region was clearly seen along the Southern shore, in the thermal images was not visible in ALGE. These patterns could be made prominent if a higher resolution grid is used. This would increase the computational time. Hence it would be appropriate to use different horizontal resolutions for different regions of the lake. The variable horizontal resolution could be integrated to ALGE without much difficulty.

- Using different weather data from the closest station for that particular region. The lake could be divided into about six regions and each region could have it's weather file from a station closest to that particular region. This would allow certain spatial features occurring due to the local weather to dominate.

- Integrate an ice model to ALGE.- It was possible to simulate the hydrodynamics for a one and a half year period continually because the lake didn't freeze the past year. Since the lake is known to freeze, an ice model has to e integrated to ALGE so that freezing of water could be taken into account.

- Radiosone data from a station close to Lake Ontario. The closest station to the lake is in Buffalo which is effected by the lake conditions of Lake Erie rather than the lake conditions of Ontario. The radiosonde station in Fort-Drum would have been more appropriate if it had been functioning for the past couple of years. The Fort-Drum radiosonde station has archive data until mid 1997.

- Integration of a biological model to ALGE.

- Simulate the years 1995 through 1997.

- Analyze weather patterns and forecast the weather for a couple of months ahead which makes it possible to predict the surface temperature of the lake.

Comparison of ALGE with images.

# Appendix A

# The contents in the attached CD

The directory

- Movie - contains some power point presentations
- Niagara - contains ALGE output of the Niagara Plume
- Plots contains all the plots that is in the thesis
- RIT-MTU - ALGE outputs compared with Temperature profiles from AVHRR Images
- RIT-OSU ALGE outputs compared with the NOAA forecasting model
- RIT-split-MTU Surface temperature from split window compared with MTU images

# Bibliography

D. Ho, A. A. and Deschamps, P. Y. (1986). Atmospheric correction for the sea surface temperature using noaa-7 avhrr and meteosat-2 infrared data. *International Journal of Remote Sensing*, 7(10):1323–1333.

Elliott, G. (1971). A mathematical study of the thermal bar. In *Proceedings 14th Conference of Great Lakes Research*, volume 14, pages 545–554. International Association of Great Lakes Research.

Elliott, G. and Elliott, J. A. (1969). Small-scale model of the "thermal bar". In *Proceedings 12th Conference of Great Lakes Research*, volume 12, pages 553–557. International Association of Great Lakes Research.

Elliott, G. and Elliott, J. A. (1970). Laboratory studies on the thermal bar. In *Proceedings 13th Conference of Great Lakes Research*, volume 14, pages 545–554. International Association of Great Lakes Research.

Farrow, D. E. (1994). An asymptotic model for the hydrodynamics of the thermal bar. *Journal of Fluid Mechanics*, 289:129–140.

Farrow, D. E. (1995). A numerical model of the hydrodynamics of the thermal bar. *Journal of Fluid Mechanics*, 303:279–295.

Garrett, A. (1997). Alge: A 3-d thermal plume prediction code for lakes, rivers and estuaries. pages 1–22.

Garrett, A. J. (1983). Drainage flow prediction with one-dimensional model, including canopy, soil and radiation parameterizations. *Journal of Climate and Appl. Meteorology*, 22(1):79–91.

Huang, J. C. K. (1972). The thermal bar. *Geophysical Fluid Dynamics*, 3:1–25.

I. A. Bychkova, S. V. V. and Demina, M. V. (1989). Use of regular ir satellite data to investigate thermal bar and upwelling phenomena. *Oceanology*, 29(5):580–584.

J. W. Budd, W. C. K. and Maclean, A. L. (1998). Documenting complex surface temperature patterns from advanced very high resolution radiometer (avhrr) imagery of saginaw bay, lake huron. *Journal of Great Lakes Resources*, 24(2):582–594.

K Fuller, H. S. and Witting, J. (1995). *The Great Lakes -An Environmental Atlas and Resource Book.* 3. Government of Canada and United Sates Environmental Protection Agency, Toronto, Ontario and Great Lakes National Program Office, Chicago, Illinois. ["http://www.cciw.ca/glimr/data/great-lakes-atlas/intro.html"].

Kosmakov, I. V. (1988). Thermal bar in the krasnoyarsk reseroir. *Meteorologia i Gidrologiya*, 3:100–109.

Kreyman, K. D. (1989). Thermal bar based on laboratory experiments. *Oceanology*, 29:695–697.

Malm, J. and Jonsson, L. (1993). A study of the thermal bar in lake ladoga using water surface temperature data from satellite images. *Remote Sensing Environment*, 44:35–46.

Mellor, G. L. and Yamada, T. (1982). Development of turbulence closure model for geophysical fluid problems. *Rev. Geophys. Space Phys.*, 20(4):851–875.

Monaldo, F. (1997). *Primer on the Estimation of Sea Surface Temperature Using TeraScan Processing of NOAA AVHRR Satellite.* The John Hopkins University.

Rodgers, G. (1971). Field investigation of the thermal bar in lake ontario: Precision temerature measurements. In *Proceedings 14th Conference of Great Lakes Research*, volume 14, pages 618–624. International Association of Great Lakes Research.

S. S. Zilitinkevich, K. D. K. and Terzhevik, A. Y. (1992). The thermal bar. *Journal of Fluid Mechanics*, 236:27–42.

Schott, J. R. The role of remotely sensed data in studies of the thermal bar.

Schott, J. R. (1982). An application of heat capacity mapping mission data thermal bar studies of lake ontario. *Journal of Applied Photographic Engineering*, 8(3).

Schott, J. R. (1997). *Remote Sensing, The Image Chain Approach.* Oxford University Press, New York.

Schwab, D. J. and Beletsky, D. (1998). *Lake Michigan Mass Balance Study: Hydrodynamic Modeling Project.* Great Lakes Environmental Research Laboratory, Michigan.

Yamada, T. (1983). Simulation of nocturnal drainage flows by a $q^2l$ turbulence closure model. *Journal of Atmospheric Science*, 40(1):91–106.